ORNL-3079
UC-80 – Reactor Technology
TID-4500 (16th ed.)

Contract No. W-7405-eng-26

REACTOR DIVISION

HFIR HEAT-TRANSFER STUDIES OF TURBULENT WATER FLOW IN THIN RECTANGULAR CHANNELS

W. R. Gambill and R. D. Bundy

DATE ISSUED
JUN 19 1961

OAK RIDGE NATIONAL LABORATORY
Oak Ridge, Tennessee
operated by
UNION CARBIDE CORPORATION
for the
U. S. ATOMIC ENERGY COMMISSION

DISCLAIMER

CONTENTS

HFIR HEAT-TRANSFER STUDIES OF TURBULENT WATER FLOW IN THIN RECTANGULAR CHANNELS

W. R. Gambill and R. D. Bundy

Abstract

In support of the High Flux Isotope Reactor program, experimental determinations were made of friction factors, burnout heat fluxes, and average and local nonboiling heat-transfer coefficients for forced-convection flow of water through thin aluminum and nickel rectangular channels under the following conditions: heat flux = 0.1×10^6 to 7.4×10^6 Btu/hr·ft^2, velocity = 10 to 85 fps, Reynolds number = 9,000 to 270,000, pressure = 1 to 39 atmospheres absolute, flow gap = 0.043 to 0.057 in., and heated length = 12 and 18 in. A few tests were made to ascertain the effect of an axially oriented cylindrical spacer strip on surface temperature distribution and burnout heat flux.

The results of these studies, unlike those of some earlier investigations of narrow-gap heat transfer, are in reasonably good agreement with accepted correlations. The friction factors are in satisfactory agreement with the Moody chart for the relative roughness of the test sections used, the burnout heat fluxes are well reproduced by the Soviet Zenkevich-Subbotin correlation, and the local and average heat-transfer coefficients are slightly larger than values predicted by the Hausen and Sieder-Tate equations.

Miscellaneous experimental and analytical HFIR heat-transfer studies not described in a previous report on the natural-circulation work,* or in the body of this report, are included in the Appendices.

Introduction

During the preliminary design of the High Flux Isotope Reactor (HFIR),[1] some consideration was given to the possible influence of the proposed narrow fuel-plate spacing (~0.050 in.) on the heat-transfer coefficients, burnout heat fluxes, and friction factors characterizing the core's thermal behavior. Of particular concern were the heat-transfer coefficients

*W. R. Gambill and R. D. Bundy, Burnout Heat Fluxes for Low-Pressure Water in Natural Circulation, ORNL-3026 (Dec. 20, 1960).

reported by Levy et al.[2] for forced-convection flow of water through rectangular channels (0.1 × 2.5 in.) heated around the entire periphery. Over the range $10^4 < (Re)_b < 10^5$,* these data fall 30 to 50% below values given by the accepted Sieder-Tate correlation.[3] Of further concern was the unusually extreme dependence of friction factors on minor surface roughness, as reported by Lancet[4] for turbulent air flow through channels with 23- to 25-mil flow gaps. Although the surface of one of Lancet's test sections was sufficiently polished (3 to 6 μin. roughness) to render it nearly hydraulically smooth by normal criteria of relative roughness, Lancet reported friction factors at $Re = 4 \times 10^4$ which are approximately double those characteristic of a smooth duct. Of final concern was the possibility that coalescence of vapor bubbles across the narrow flow gap might produce burnout at lower-than-normal heat fluxes.

Since the thermal performance level of the HFIR will be high, it was decided to resolve these uncertainties by conducting a limited number of experimental determinations of the pertient heat-transfer parameters. The studies, which extended over a nine-month period, resulted in the recommendation of correlations which were used in the final thermal design of the HFIR core.

Experimental Program

System Description

The experimental system, depicted schematically in Fig. 1, was a modification of that used previously for swirl-flow heat-transfer experiments.[5] The coolant water (distilled in all but the earliest tests) was pumped from a 300-gal holdup tank through the indicating rotameters and booster pumps and into the vertical test section. The holdup tank, Unichrome lined to prevent water contamination, also served as a weigh tank for rotameter calibration. The mixing chamber was of disk-and-donut construction, the thermocouples were Chromel vs Alumel, and all piping (except in the earliest experiments) was type 304 stainless steel. A

*See section on Notation for definition of terms.

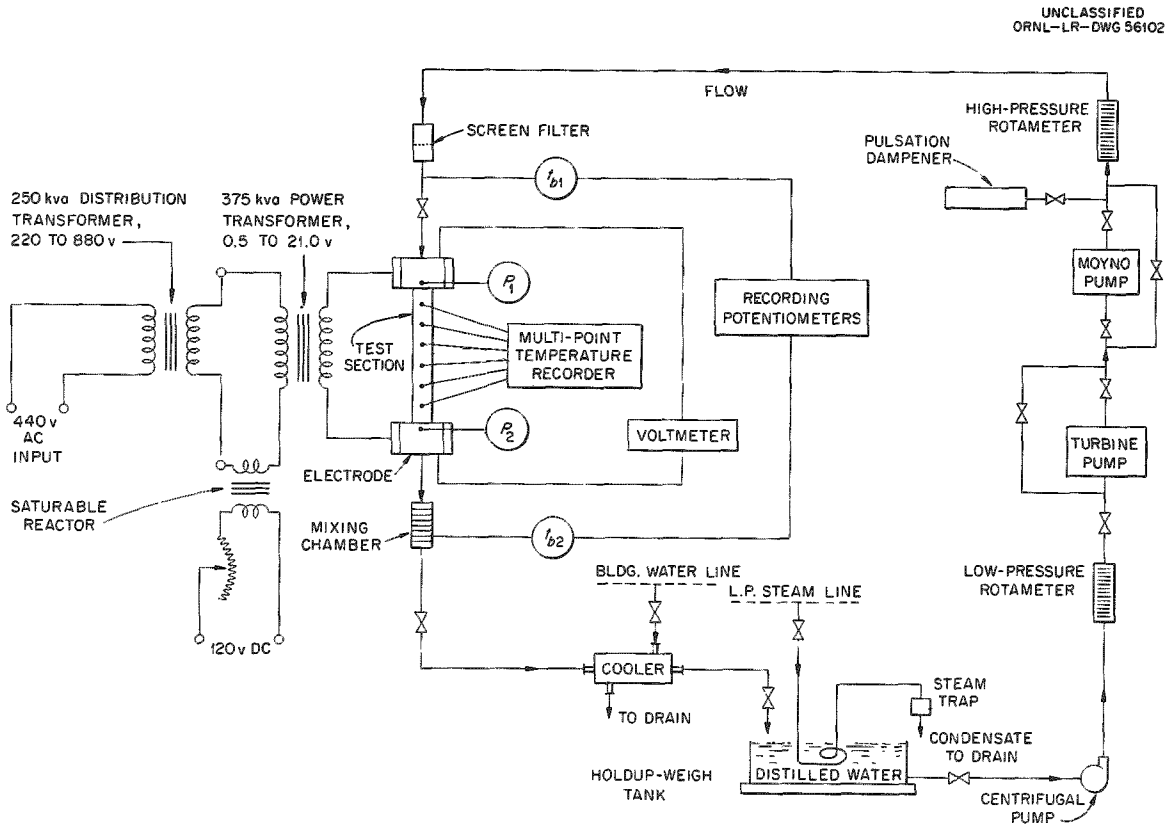

Fig. 1. Experimental Heat-Transfer System.

wire-screen filter was placed in the piping upstream of the test section. In order to prevent coolant flashing upon pressure letdown at the weigh tank, a two-pass, shell-and-tube cooler was inserted upstream of the tank. Static coolant pressures at stations P_1 and P_2 were read on calibrated Heise gages during steady-state operation, and were taken from a Sanborn high-speed recorder trace for the burnout reading. The test section was enclosed in a shield box welded from 1/4-in. mild steel; the shield was intended to protect personnel from flashing steam at burnout and possibly from a violent Al-H_2O explosion (which did not materialize). The inlet water temperature was adjusted with a steam-heated coil fabricated of 1/2-in.-diam stainless steel tubing located in the holdup tank. The test section was electrically isolated from the remainder of the system with flanged connections made with tape-wrapped bolts and Teflon gaskets. Water flow through the test sections was vertically downward in all cases.

Description of Test Sections

Nickel Test Sections. Tests 1 through 3 were conducted with test sections made of 0.060-in.-thick nickel plates. In test 1, these were welded to Inconel side strips; separation of the composite plates was provided by recessed Inconel spacer strips at the edges, as shown in Fig. 2. Inconel edge and spacer strips were used in order to decrease the heat generation rate at the sides of the channel. Were this not done, premature burnout would be induced by the large impressed heat fluxes in the corners of the flow channel. The test sections were copper brazed into slotted end blocks, fabricated as shown in Fig. 3. The end blocks served as flow transitions between the terminal piping and the rectangular

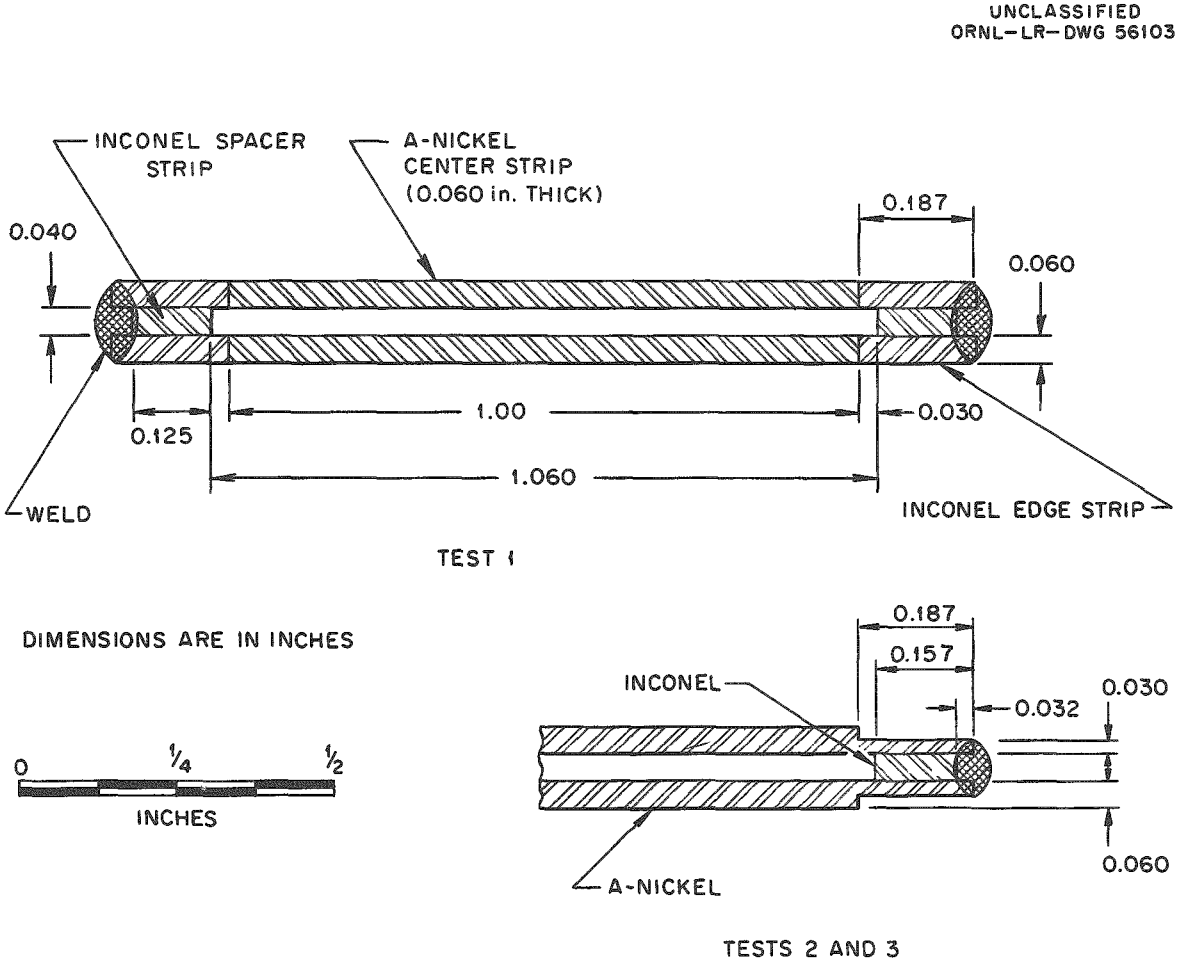

Fig. 2. Cross-Sectional View of Nickel Rectangular Test Sections.

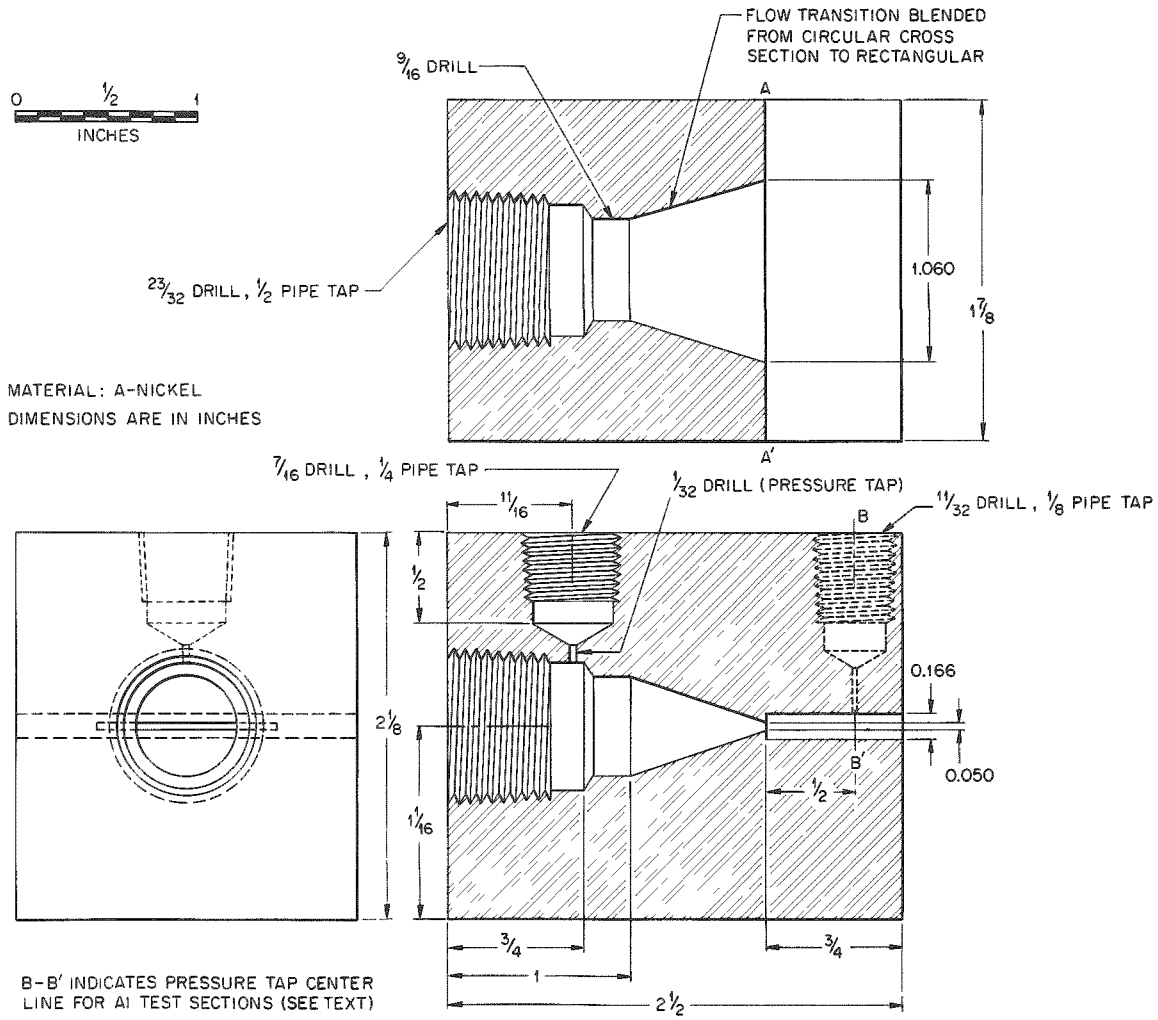

Fig. 3. End Blocks for Nickel Test Sections.

cross section of the flow channel, and as points of attachment for the static-pressure taps, voltage measuring leads, and copper electrodes. Subassembly of the flow channel and end blocks is depicted in Fig. 4, and the final assembly is illustrated in Fig. 5. The back-up plates, machined from 1-in.-thick cold rolled steel, were designed to hold the increase in flow-channel gap to considerably less than 1 mil under operating conditions.

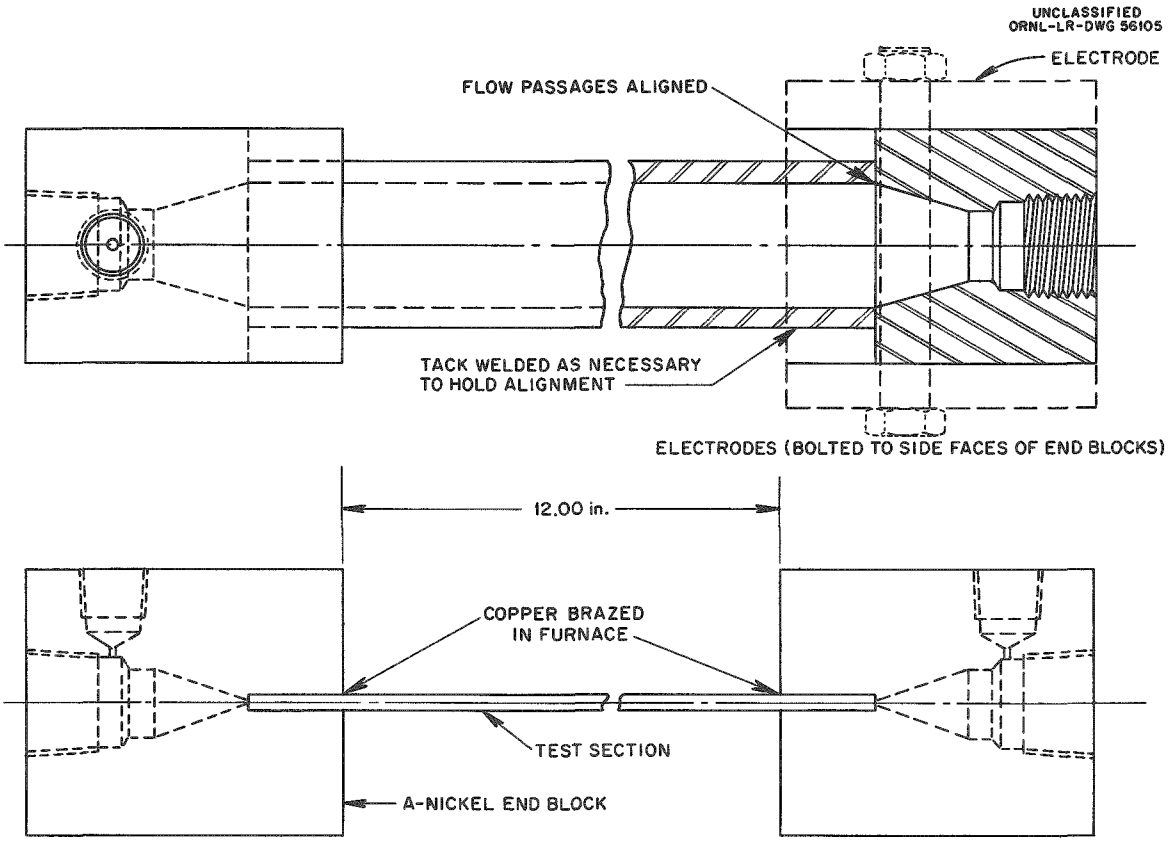

Fig. 4. Subassembly of Nickel Test Section.

Six Chromel-vs-Alumel thermocouples, alternately spaced on opposite sides of the test section, were discharge-welded to the outer surfaces of the nickel plates. Thermocouple lead wires were brought to the outside through holes in the back-up plates, as shown in Fig. 5. After the test section was assembled, two 3/8-in.-diam holes were drilled through each end block, and the electrodes were attached with stud bolts to give a tight press fit (as indicated in Fig. 4).

In order to avoid problems which arose during welding of the thin Inconel edge strips to the A-nickel center strips, test sections for tests 2 and 3 were fabricated with solid A-nickel plates, with a 0.187-in. width of each edge milled to a thickness of 0.030 in. (see Fig. 2). This construction, which equally well decreases heat generation at the sides of the flow channel, is similar to the design used by Westinghouse in their high-pressure bulk-boiling burnout tests.[6] The test-section dimensions are tabulated in Tables 2 and 3 of subsequent sections of this report.

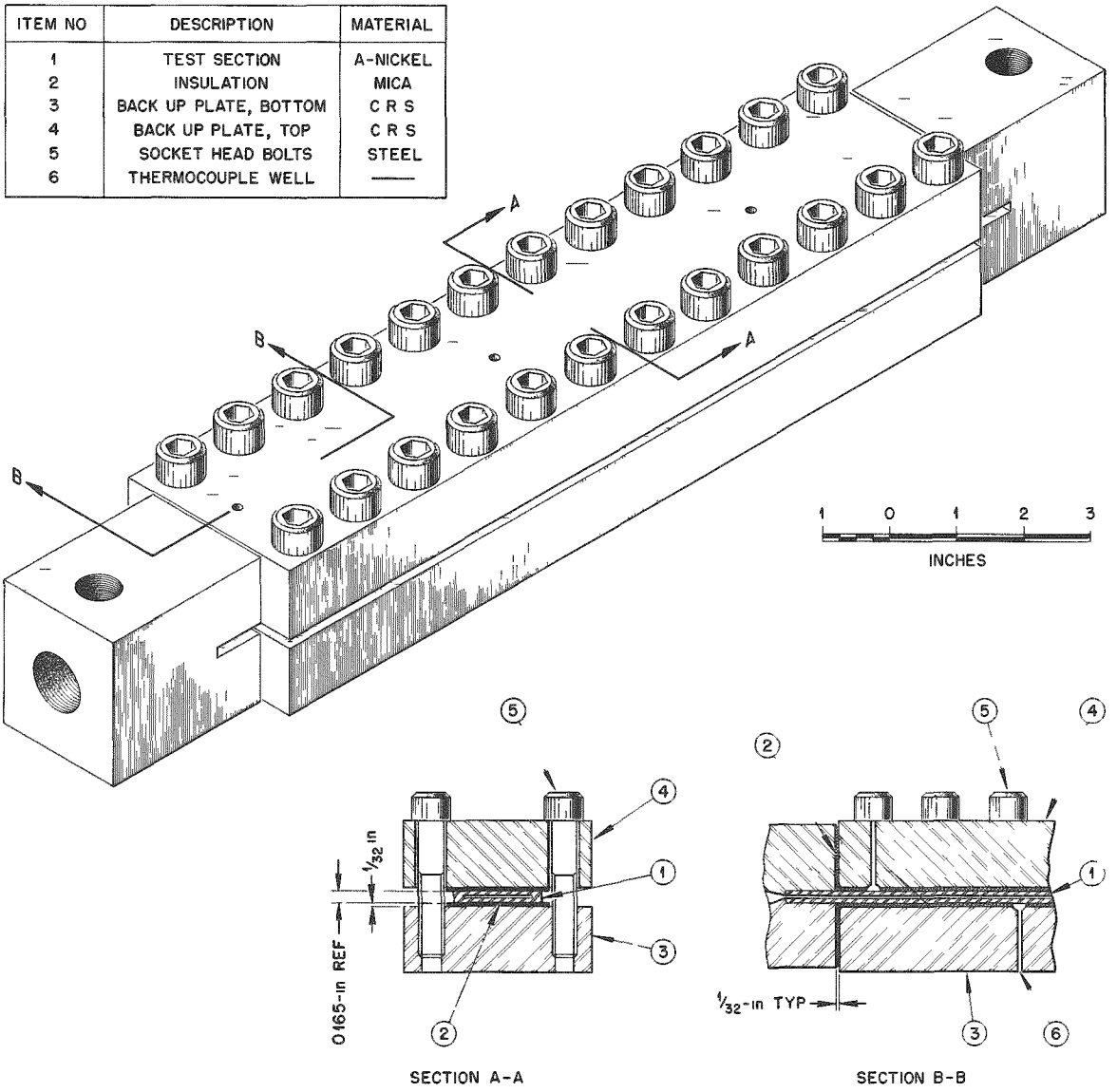

Fig. 5. Nickel Test Section Assembly.

In copper-brazing the end-block joint for the second test section, some difficulty was encountered because of the change in cross section; the third set of end blocks was consequently modified by cutting, by the Elox process, a 1/8-in.-deep recess (to the left of line A-A′ of Fig. 3) to conform to the new cross section of the test section.

Aluminum Test Sections. Tests following test 3 were conducted with aluminum test sections for three reasons: (1) to decrease the temperature

drop between the outer and inner surfaces of the heated wall, thus increasing the reliability of the derived heat-transfer coefficients, (2) to better match the characteristics of the electrical system with an 18-in. heated length (which was specified for the HFIR core at about this time), and (3) to determine whether aluminum, which will be used for the reactor fuel-plate cladding, gives burnout results in agreement with those obtained with nickel surfaces.

Since no direct method of joining a higher resistance material to aluminum appeared feasible, an alternate design for preventing heat-flux peaking around the edges of the flow channel became necessary. The problems involved in maintaining a nearly constant heat flux around the periphery of the flow channel are delineated in Fig. 6, where it is shown

UNCLASSIFIED
ORNL-LR-DWG 56107

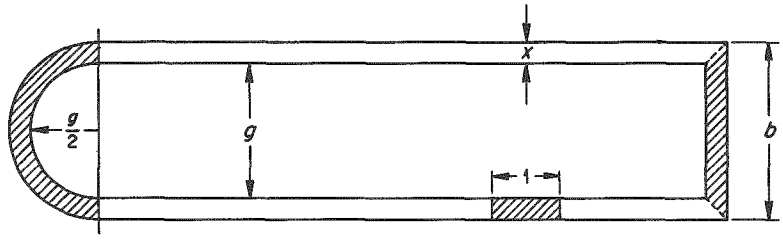

CONSTANT x, UNIT DEPTH, SEMICIRCULAR CROSS SECTION AT CURVED EDGE.

CURVED	FLAT	RIGHT ANGLE
$A_h = (\pi)(\frac{g}{2})(1) = \frac{\pi g}{2}$	$A_h = 1$	$A_h = g$
$V_h = \frac{\pi[(\frac{g}{2}+x)^2 - (\frac{g}{2})^2]}{2}$	$V_h = x$	$V_h = \frac{x}{2}(g+b)$
$V_h = \frac{\pi x}{2}(g+x)$	$\frac{V_h}{A_h} = x$	$b = g + 2x$
$\frac{V_h}{A_h} = \frac{x(g+x)}{g}$		$V_h = x(g+x)$
		$\frac{V_h}{A_h} = \frac{x(g+x)}{g}$

$$\frac{(V_h/A_h)_{CURVED}}{(V_h/A_h)_{FLAT}} = \frac{(V_h/A_h)_{RIGHT\ ANGLE}}{(V_h/A_h)_{FLAT}} = \frac{g+x}{g}$$

Fig. 6. Peripheral Heat-Flux Variation for a Rectangular Test Section of Constant Wall Thickness.

that for a constant wall thickness, the electrically heated volume per unit internal surface area is given, for either a semicircular or right-angle edge, by the sum of the flow gap and wall thickness divided by the flow gap. Since

$$\phi = \frac{q}{A_h} = \frac{q}{V_h}\frac{V_h}{A_h} ,$$

$\phi \propto V_h/A_h$ if q/V_h is constant. For the dimensions of the aluminum test sections (g = 50 mils and x = 35 mils), the heat flux at the sides of the flow channel would peak by a factor of 1.7, were x constant.

A similar analysis for a rectangular channel with unequal flat and curved wall thicknesses (see Fig. 7) yields a relation for approximating the curved-wall thickness necessary for a uniform peripheral heat-flux distribution. If g = 50 mils and x_b = 35 mils, the final equation given in Fig. 7 indicates that x_a must be 24 mils if ϕ_a/ϕ_b is to be unity. These dimensions were used in making a number of aluminum test sections, which were fabricated by rolling a soft type 1100 aluminum tube of the appropriate wall thickness onto a lubricated, hard-rubber mandrel of rectangular cross section with semicircular edges, following which the insert was withdrawn and a round-edged sizing disk pushed through. The final dimensions (tabulated in Table 3) were sufficiently close to those specified and quite consistent among the test sections used.

Also changed for the aluminum test series was the location of the terminal static-pressure taps, which were moved to B-B′ of Fig. 3 in order to avoid reliance on somewhat uncertain end-loss corrections for friction-factor calculations. The pressure-tap hole at B-B′ was not initially completed through the test-section wall, since it could have become plugged during the subsequent brazing operation. After furnace brazing with Eutectic 190 compound, the hole was extended through the test-section wall by an electrical-discharge machining technique (Elox process), which leaves no interior metal burr to disturb the flow pattern about the measurement point. The end blocks in these tests were also made of type 1100 aluminum.

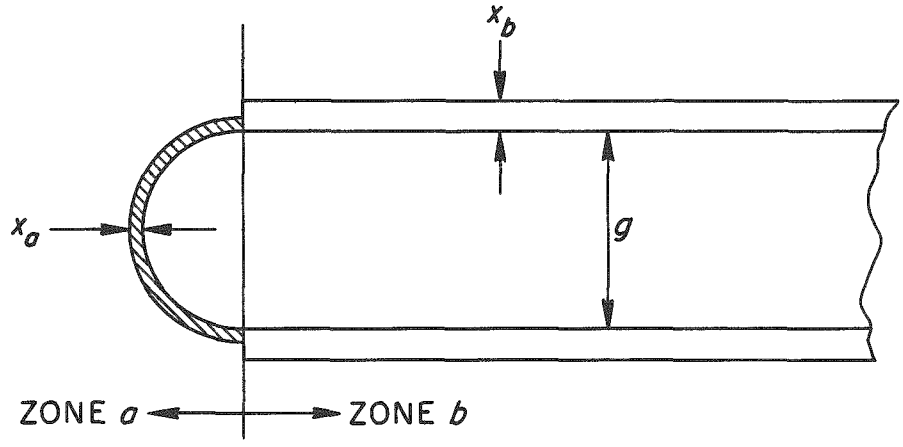

$$I = E/R;\ R = \rho L/A_x;\ I = EA_x/\rho L;\ \frac{I_a}{I_b} = \frac{(A_x)_a}{(A_x)_b}$$

$$q_a/q_b = E_a I_a/E_b I_b;\ E_a = E_b;\ q_a/q_b = (A_x)_a/(A_x)_b$$

$$\phi = q/A_h;\ \therefore \phi_a/\phi_b = \frac{(A_x/A_h)_a}{(A_x/A_h)_b}$$

ZONE a	ZONE b
$A_x = \frac{\pi x_a}{2}(g + x_a)$	$A_x = (x_b)(1) = x_b$
$A_h = \pi g/2$	$A_h = 1^2 = 1$
$\therefore (A_x/A_h)_a = \frac{x_a(g + x_a)}{g}$	$\therefore (A_x/A_h)_b = x_b$

$$\phi_a/\phi_b = \phi_{CURVED}/\phi_{FLAT} = \frac{x_a(g + x_a)}{g\,x_b}$$

Fig. 7. Peripheral Heat-Flux Variation for a Rectangular Test Section with Unequal Flat and Curved Wall Thicknesses.

Rather than natural mica, machined Mycalex (a high-temperature bonded form of synthetic mica) was used for electrical isolation of the back-up plates from the end blocks and test section. Since the thermocouples (36-gage Chromel vs Alumel) could not be reliably attached to the aluminum test section by discharge welding, as with nickel, a press contact was used — as depicted in the insert of Fig. 8, a longitudinal section of the

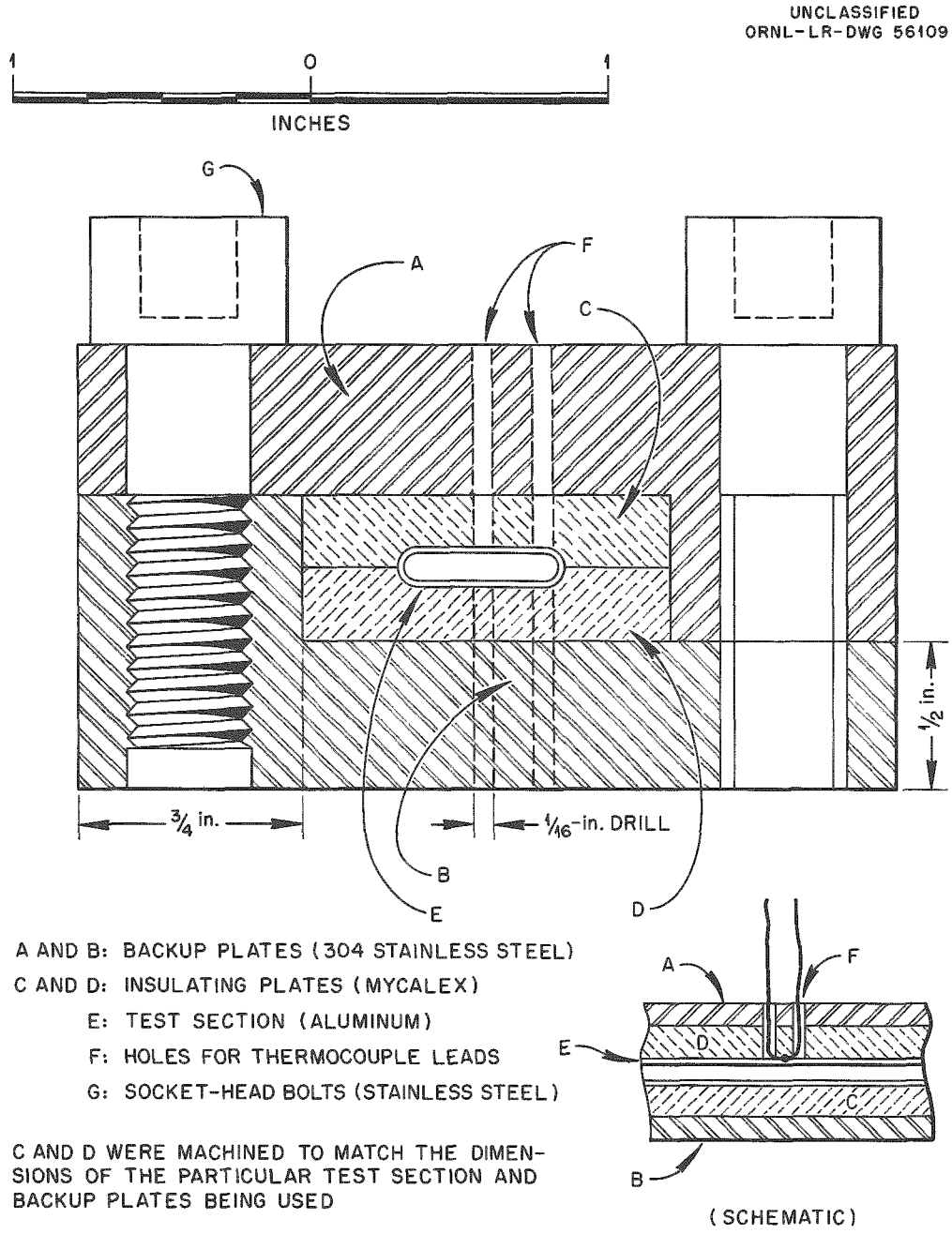

Fig. 8. Cross Section of Aluminum Test-Section Assembly.

assembly. Internal coolant pressure during a test expanded the aluminum wall slightly to cause a partial embedding of the thermocouple bead in the surface; traces of this indentation were visible after test-section disassembly. A total of 12 thermocouples was used in each test, with stations spaced nominally at 2-in. axial intervals on alternately opposing sides of the test section. At four stations, a thermocouple was also placed at the edge of the flat portion of the aluminum wall to obtain data on the lateral temperature distribution (see Fig. 8). The calculated maximum increase of flow gap permitted by the 1/2-in.-thick, type 304 stainless steel back-up plates was 1.17 mils under operating conditions of 500°F (back-up temperature) and 600 psia (water pressure).

An aluminum test section is shown in various stages of assembly in Figs. 9 through 13. Figure 11 gives an indication of the excellent (and typical) congruency obtained between test section and Mycalex insulators.

Aluminum Test Sections with Axial Spacers. Four tests were conducted with centered spacer strips of slightly flattened cylindrical cross section running the length of the flow channel. The spacers were made by lightly rolling 0.056-in.-o.d. stainless steel tubing (6-mil wall) until the dimension across the flats was nominally 50 mils. The spacers were slotted at the ends to allow thermal expansion, pulled through the flow channel, and then centered laterally by 30-mil pins inserted through both channel wall and spacer-tube slot at each end of the test section. The spacer tube was then closed off at the ends, placed under tension, and welded to cross pins placed in the terminal piping attached to the end blocks. Since the spacer occupied the center of the flow channel, the pressure taps were moved laterally until their centerlines were midway between the edge and the center of the flow channel. Thermocouples were grouped in threes at each end of the test section, one directly over the spacer, and one at each side of the central thermocouple. At each of three intermediate thermocouple stations, two thermocouples were used, one over the spacer and one to the side. There were thus five stations at nominal 3-in. intervals, involving a total of 12 thermocouples. Final spacer dimensions are given in Table 1.

Net flow areas, equivalent diameters, and heated surface areas for all test sections are tabulated in Table 2, as calculated from dimensions

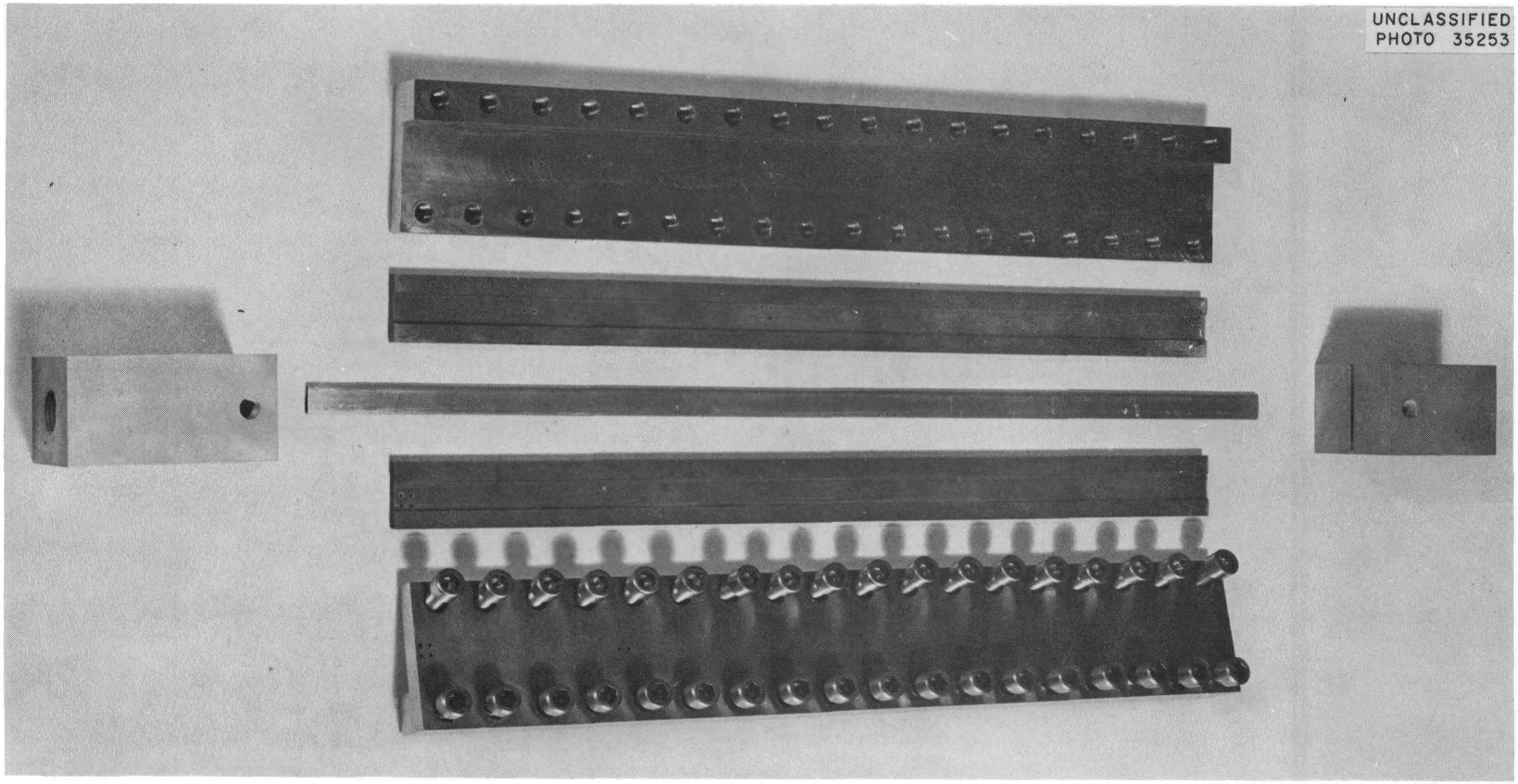

Fig. 9. Basic Components of Aluminum Test-Section Assembly. Top to bottom: backup plate, Mycalex insulator, test section and end blocks, Mycalex insulator, and backup plate.

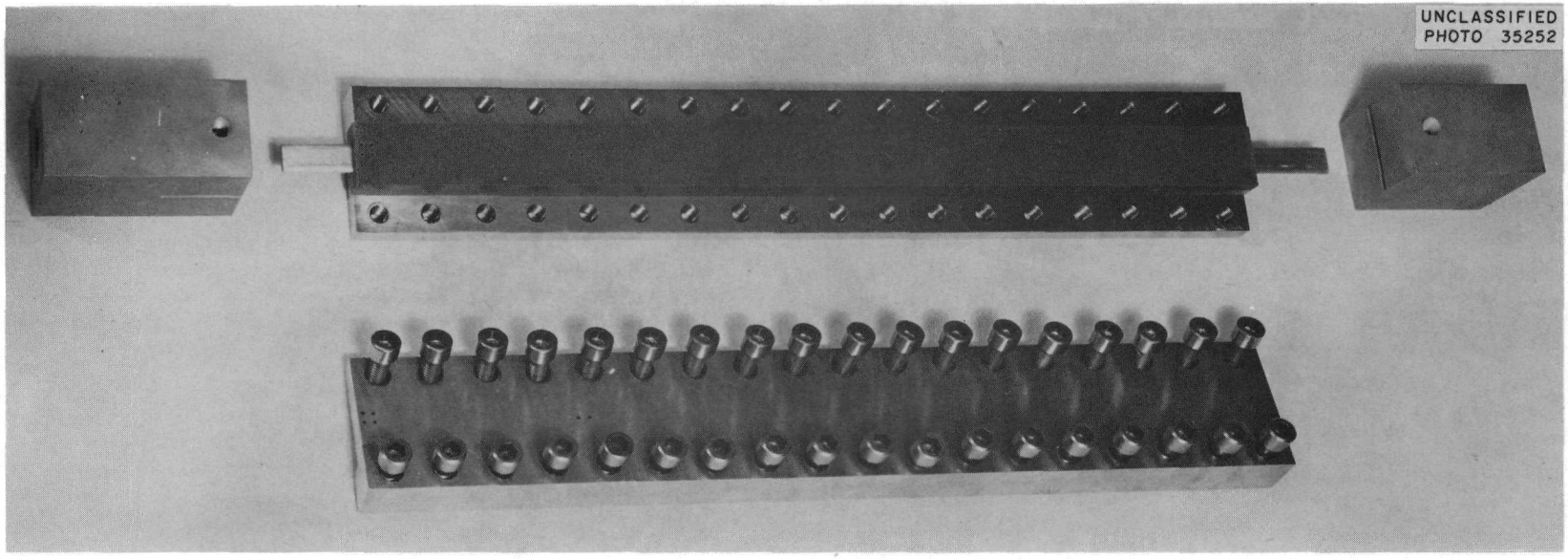

Fig. 10. Aluminum Test Section Enclosed in Mycalex Insulator.

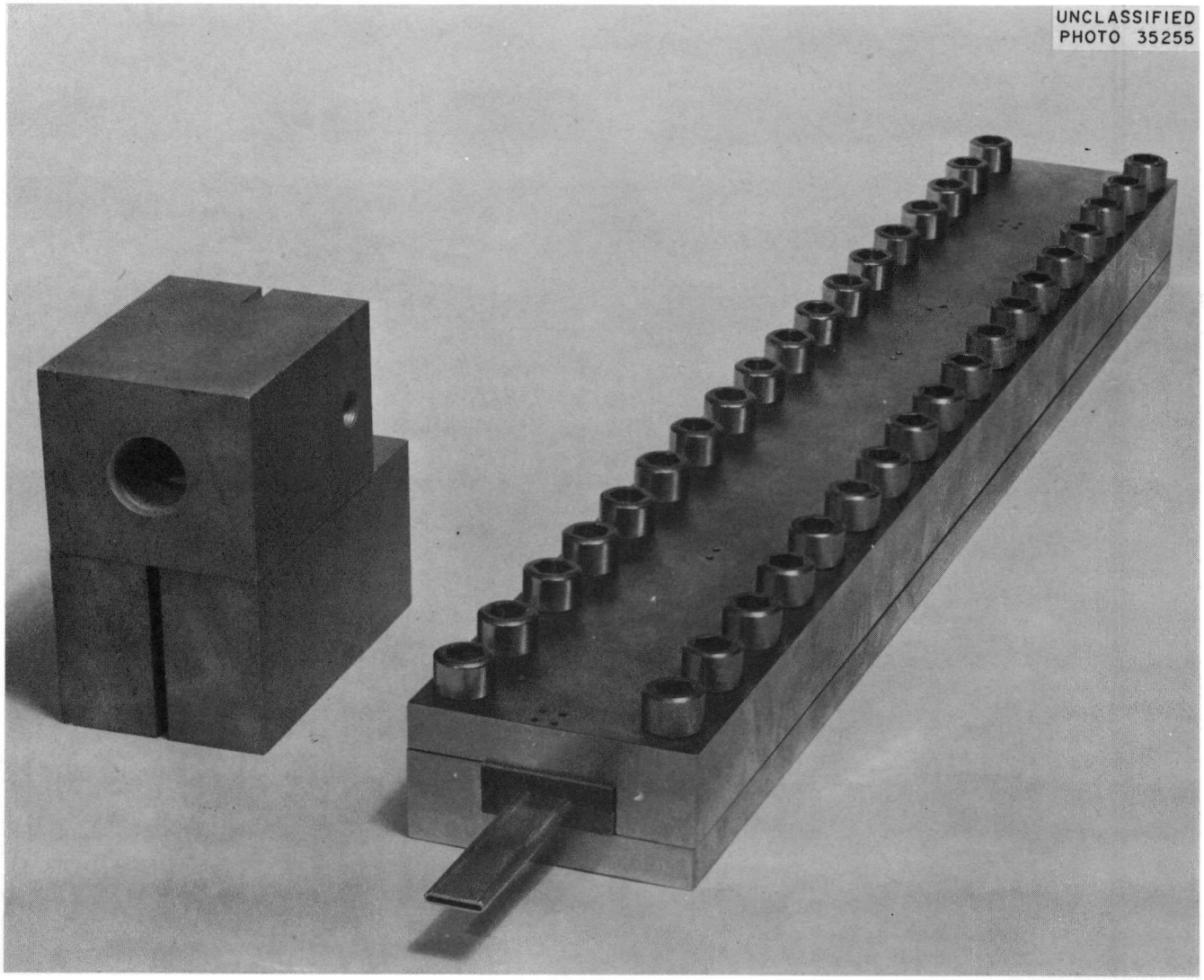

Fig. 11. Previous View with Backup Plates Added. End blocks show end receiving pipe (top) and test section (bottom).

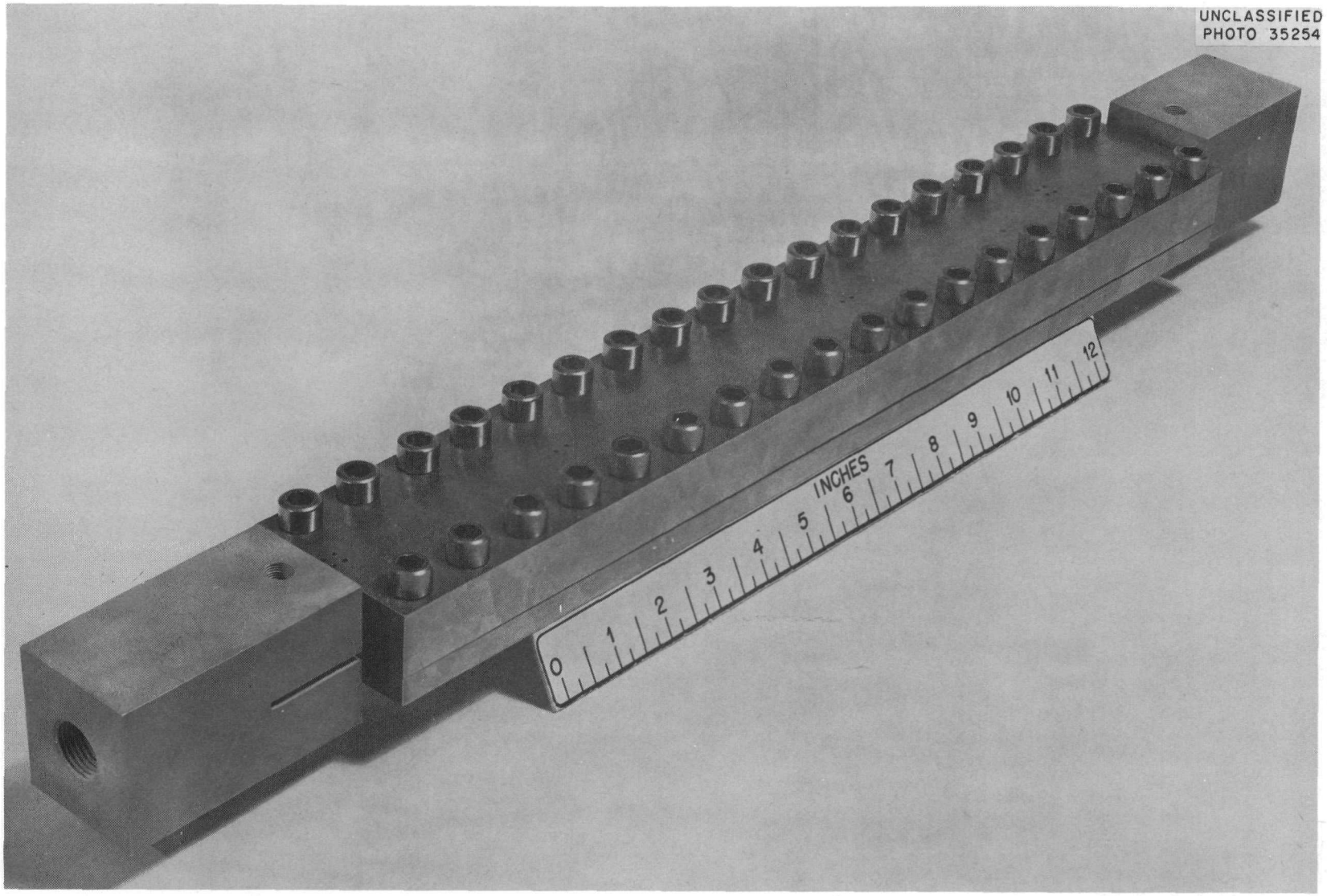

Fig. 12. Completed Aluminum Test Section Assembly. Pressure taps may be seen at tops of end blocks.

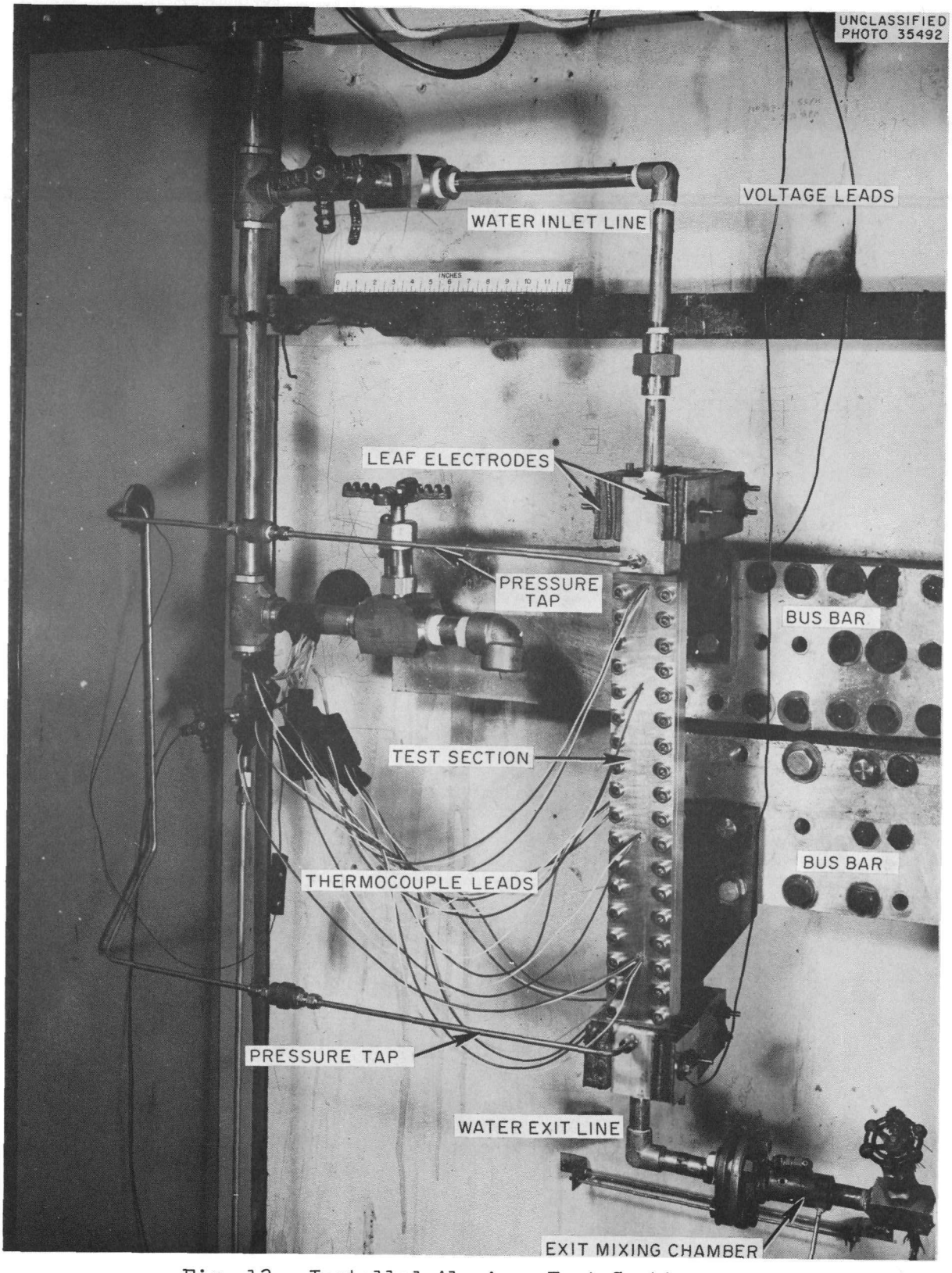

Fig. 13. Installed Aluminum Test Section.

Table 1. Spacer Dimensions[a] for Tests 8 Through 11

Test No.	h_s (in.)	W_s (in.)	g_s (in.)
8	0.048	0.067	0.008
9	0.046	0.069	0.004
10	0.054	0.059	0.001
11	0.052	0.061	0.001

[a]Determined after termination of test.

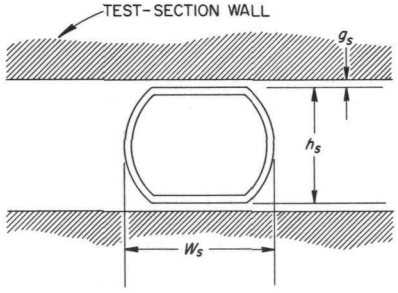

Table 2. Net Flow Area, Equivalent Diameter, and Heated Surface Area for All Test Sections

Test No.	a_f (in.^{2})	D_e (in.)	A_h (ft^2)
1	0.0457	0.0827	0.1668
2	0.0470	0.0863	0.1685
3	0.0527	0.0938	0.1667
4	0.0258	0.0978	0.1341
5	0.0267	0.0995	0.1360
6	0.0267	0.0994	0.1356
7	0.0278	0.1045	0.1352
8	0.0279	0.0920	0.1381
9	0.0229	0.0750	0.1349
10	0.0247	0.0808	0.1386
11	0.0235	0.0773	0.1328

measured after test termination. When the measurements at the burnout site differed significantly from the average value for the entire test section (two instances), the average value was used in reducing the heat-transfer data and the local value was used in burnout calculations. The

equivalent diameter was taken as four times the net flow area divided by the wetted perimeter. The presence of the spacer was accounted for in calculating a_f and D_e for tests 8 through 11, but A_h was calculated as if the spacer were not present. This approach is justified by consideration of two possible cases: if the spacer did not touch the test-section wall, the heat flowed from the aluminum surface into the water film, as with no spacer; and if the spacer did touch the wall, the heated area was still essentially the same, since the spacer was approximately square and the covered wall area was approximately equal to the area of the sides of the spacer strip.

Operating Procedure

During each test, the outside wall temperatures were allowed to equilibrate a number of times before burnout. Data suitable for calculation of heat-transfer coefficients and friction factors were collected during these periods of steady state operation. Little time was required for equilibration because of the generally high heat fluxes and film coefficients and the relatively small heat capacity of the test section. The physical operations performed during preparation of a test section and following burnout are listed below:

Channel Measurements Before Brazing

1. Measure inside width and thickness
2. Measure outside width and thickness
3. Adjust heated length to 12 or 18 in.

After Brazing

1. Drill or Elox pressure-tap holes through channel
2. Install voltage-tap lugs
3. Remove pressure-tap burrs from inner surface (when drilled)
4. Clean tube interior
5. Measure outside width and thickness
6. Measure heated- and voltage-tap lengths
7. Measure water condition (pH and electrical resistivity)

After Test

1. Check thermocouples for tightness
2. Measure burnout location
3. Measure water condition
4. Measure channel outside width and thickness at several axial positions
5. Measure channel inside width and thickness at several axial positions
6. Measure wall thickness at several axial positions
7. Examine inner wall for deposits at several positions
8. Determine interior surface roughness with profilometer at several axial positions

Ranges of Conditions

The heat flux was varied from 0.1×10^6 to 7.4×10^6 Btu/hr·ft^2, the exit coolant pressure from 1.1 to 38.6 atmospheres absolute, the heated length from 12.0 to 18.8 in., and the flow-channel equivalent diameter from 0.075 to 0.105 in. Velocities ranged from 10.2 to 85.4 fps, corresponding to local Reynolds numbers from 9.0×10^3 to 2.7×10^5. Both aluminum and nickel test sections were used, and the after-test surface roughnesses varied from 45 to 200 μin. rms. Local heat-transfer coefficients ranged from 3120 to 38,200 Btu/hr·ft^2·°F, and burnout heat fluxes from 3.04×10^6 to 7.36×10^6 Btu/hr·ft^2.

Results and Discussion

Data pertinent to the eleven tests are given in Table 3. The last column of Table 3 and all of Table 4 relate only to the conditions at burnout, with which each test was terminated. Since existing correlations for f, h, and ϕ_{bo} are generally supported by many data obtained in other studies, it was felt that selection of the existing equation which best represents the new data would lead to more reliable recommendations than development of new correlations based only on the present data.

Table 3. Forced-Convection Burnout Test Conditions

Test No.	Test Section							Water Condition[a,b]		t_{b_1} (°F)
	Material	L_h (in.)	Flow Gap (in.)[a]	Gap Width (in.)[a]	x (in.)[a] Flat	x (in.)[a] Curved	ϵ (μin. rms)[a]	pH	ρ_e (ohm-cm)	
1	A-nickel plates separated by Inconel spacers	12.01	0.043	1.062	0.060	(side spacer)	200	c	c	123.8
2	"	12.13	0.045	1.044	0.060	(side spacer)	c	c	c	123.8
3	"	12.00	0.049	1.075	0.060	(side spacer)	c	c	c	129.0
4	Type 1100 aluminum	18.27	0.053	0.498	0.035	0.028	63	6.69	215,000	124.2
5	"	18.29	0.054	0.505	0.035	0.025	65	6.70	145,000	96.5
6	"	18.14	0.054	0.506	0.035	0.025	65	6.63	210,000	91.6
7	"	18.28	0.057	0.501	0.035	0.027	60–75	6.50	260,000	120.2
8[d]	"	18.53	0.064	0.500	0.035	0.026	65–75	6.86	123,000	112.4
9[d]	"	18.28	0.054	0.500	0.036	0.027	50–60	6.40	210,000	113.4
10[d]	"	18.78	0.056	0.499	0.037	0.027	45–65	6.50	205,000	116.4
11[d]	"	18.05	0.054	0.498	0.038	0.028	65–90	6.62	135,000	109.2

[a]Average value, determined after termination of test.

[b]Water pH and ρ_e determined at 23.3 to 29.5°C.

[c]Not measured.

[d]In these tests, an axially oriented, centered spacer strip of slightly flattened cylindrical cross section was used.

Table 4. Forced-Convection Burnout Test Results

Test No.	$(P_2)_{bo}$ (psia)	$(t_{b_2})_{bo}$ (°F)	$(\Delta t_{sub})_{2,bo}$ (°F)	$(V_2)_{bo}$ (fps)[a]	ϕ_{bo} (10^6 Btu/hr·ft^2)				
					Experimental		Predicted		
					Average	At Burnout Site[b]	Bernath (ref. 12)	Menegus (ref. 19)	Zenkevich-Subbotin (ref. 21)
1	560	453	26.0	31.8	3.55	3.89	3.80	3.58	2.70
2	465[c]	414	46.0	35.4	3.84	4.20	3.58	4.36	3.50
3	535	384	90.0	35.8	3.74	4.03	5.90	5.75	4.52
4	550	441	36.0	45.5	3.64	4.34	5.21	4.40	3.70
5	566	426	54.0	30.4	2.62	3.04	4.29	3.98	3.38
6	160	317	46.5	54.1	3.42	4.99	6.04	4.65	4.62
7	355	358	74.9	85.4	6.15	7.36	10.47	8.09	6.57
8[d]	521	422	49.3	38.4	3.26	3.67	5.02	4.60	3.75
9[d]	465	413	47.1	46.0	3.21	3.59	6.45	5.92	4.06
10[d]	505	404	64.0	42.5	3.01	3.25	6.69	6.12	4.28
11[d]	462	459	4.8 wt % quality	$G = 6.42 \times 10^6$	3.19	3.36	← e →		

[a]The corresponding mass velocities varied from 5.75×10^6 to 17.00×10^6 lb/hr·ft^2.

[b]Burnout occurred 1/8 to 3/8 in. upstream of the heated exit, except in one test when it occurred at 1 1/4 in. upstream.

[c]Equilibrium reading just before violent pressure fluctuation at burnout (which occurred only during this test).

[d]In these tests, an axially oriented, centered spacer strip of slightly flattened cylindrical cross section was used.

[e]Method is inapplicable when net steam is generated. The bulk-boiling correlation of ref. 14 gives $\phi_{bo} = 4.31 \times 10^6$ Btu/hr·ft^2.

Friction Factors

Thirty-two friction factors calculated for test 1 deviated (for the relative roughness of the specific channel) from the conventional Moody correlation[7] by ±13% (average) and ±46% (maximum). The results of this test gave no indication of the unusually extreme dependence of friction factor on minor surface roughness that was reported by Lancet.[4] Tests 2 and 3 gave inordinately small friction factors because of improperly located pressure taps. No f calculations were made for tests 8 through 11, since the reduction of D_e caused by the presence of the spacers in the relatively narrow (0.5 in.) experimental flow channels would not be representative of the spacer pattern and corresponding change of D_e in an HFIR core.

The majority of the friction-factor data were obtained during tests 4 through 7, which were characterized by a relative surface roughess (ϵ/D_e) of $\sim 6.4 \times 10^{-4}$. In these tests, the pressure taps were made through the wall of the test section in order to avoid terminal pressure-drop corrections for f calculations and to obviate possible influences of turbulence generated by the upstream end-block threads.

The results of these tests — 66 points, all under nonboiling conditions — are shown in Fig. 14 as the isothermal friction factor versus the bulk Reynolds number. The bulk-to-wall viscosity factor, 1.02 $(\mu_b/\mu_w)^{0.14}$, is ordinarily included in the friction-factor equation when heat is exchanged in order to account for changes in the turbulent velocity profile of the fluid. The displacement of the present results from heated-test results increased, however, when this factor was used, that is, the heated-run data, when converted to an isothermal basis, fell farther above the isothermal data than when the ratio was omitted.

Some confirmation of the agreement of the present friction factors with conventional correlations may be found in a Westinghouse study,[8] in which three points are reported for smooth 53-mil flow gaps at Reynolds numbers of 5×10^4 to 2×10^5. In this case, the points fell within ±10% of the usual Moody curve. It was also reported that for all gap thicknesses at $Re \leq 10^5$, there was no effect of surface roughness over the range $6 < \epsilon < 25$ μin.

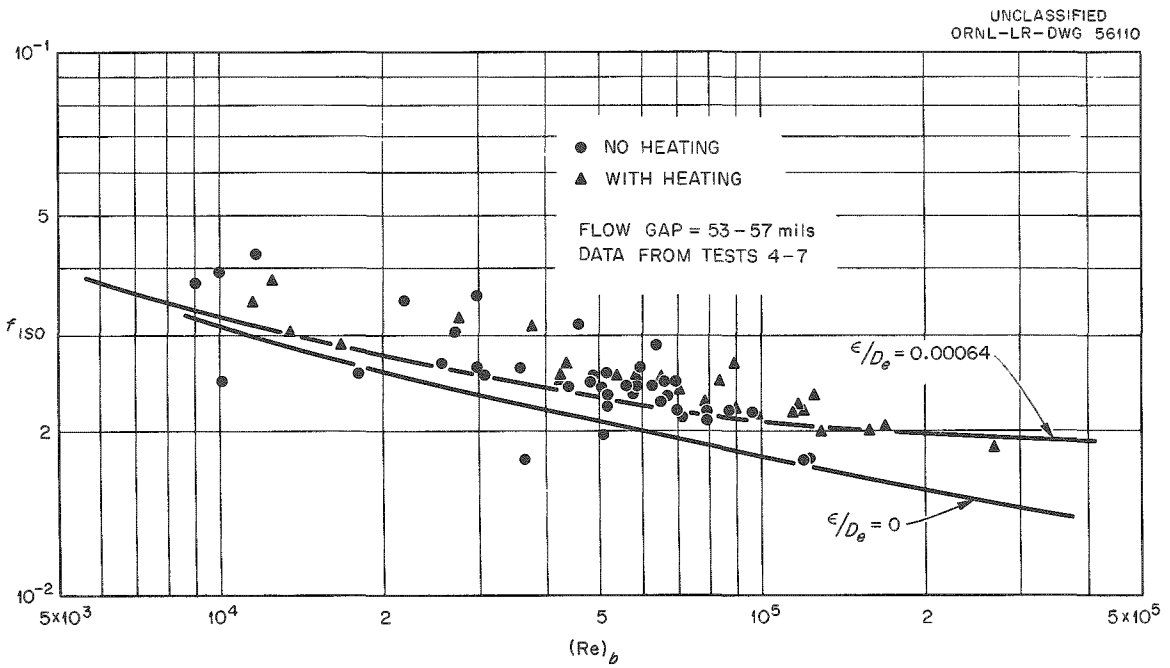

Fig. 14. Friction-Factor Data for Thin Rectangular Channels.

A dimensional uncertainty of 0.001 in. in a flow gap of 0.050 in. corresponds to an uncertainty of 6.1% in the friction factor and a 2-mil uncertainty to 12.8%. The dimensional tolerances of the test sections and the data scatter in Fig. 14 combine to justify a design recommendation for f of

$$f_{HFIR} = 1.15\, f_{Moody,\ iso} \qquad (1)$$

Of all the data points, 85% fall on or below this recommendation.

Burnout Heat Fluxes

Review of Other Studies. Data on burnout heat fluxes for water flowing through thin rectangular channels at low and moderate pressures are sparse. Westinghouse workers have reported their results[9] for flow gaps of 50 to 101 mils, but these tests were conducted primarily at 2000 psia under conditions of net steam generation.

Levy and co-workers[2] reported data for water at 65 to 138 psia flowing at 6 to 53 fps through 0.118 × 2.405-in. test sections. In these

studies, heat production rates in the corners of the test sections were high, in simulation of what would be extraordinarily intense gamma and neutron side-plate heating, and burnout occurred at the corners at heat fluxes approximately one-third those characteristic of circular pipes. Since, in this case, the heat flux peaked in the corners, a comparison of the actual local flux with the predicted burnout flux would be more pertinent than the comparison of channel-average and predicted burnout fluxes which was used. In illustration, the results of a Westinghouse investigation[10] may be cited wherein the ratio of edge to flat-face heat fluxes was varied from 1.34 to 2.05 by altering the thickness of the heated metal at the narrow face. The WAPD burnout equations[9] predicted burnout fluxes as much as 60% greater than the experimental values of mean flat-face flux at burnout, but the agreement between prediction and experiment was within the usual ±35% when the peak value of edge heat flux, estimated by an electrical analog method, was used.

A single test reported in the literature[11] gave an early indirect indication that flow gaps can be reduced to very small dimensions without strongly influencing the burnout heat flux. In the test reported, a maximum heat flux of 7.9×10^6 Btu/hr·ft^2 was attained (without burnout) when 15°C water was pumped at 51.6 fps through two parallel flow channels, each $0.010 \times 0.197 \times 0.787$ in. If the exit coolant pressure, not stated in the paper, is taken as atmospheric, Bernath's extended burnout correlation[12] predicts a ϕ_{bo} of 11.7×10^6 Btu/hr·ft^2 for this case, so the operating heat flux reached approximately two-thirds of the predicted burnout value without failure, although the gap was only 10 mils.

Most pertinent to the problem of flow-gap effects on ϕ_{bo} is the study of Kafengauz and Bauarov,[13] which was encountered toward the close of the present investigation. Subcooled water at 40 atm was pumped upward through vertical rectangular nickel test sections of 2-in. length at velocities of 3.0 to 88.5 fps. The flow gap was incrementally reduced from 79 to 8 mils, and no effect on burnout was noted for gaps larger than ~28 mils. At the minimum gap of 8 mils, the effect was maximum, that is, burnout occurred simultaneously with the initiation of local boiling. In contrast, for all flow gaps greater than ~28 mils, the ϕ_{bo} was ~3.6

times the heat flux at initiation of local boiling. The results of this study strongly indicate that gap dimensions do not influence the ϕ_{bo} until the gap is decreased to a size comparable to maximum bubble diameters.

Present Investigation, Channels Without Spacers. The burnout results of the present study are outlined in Tables 3 (test conditions) and 4 (test results). The heat flux at the burnout site was obtained from the average heat flux measured at burnout by multiplying by the ratio of the electrical resistivities at the measured exit and average surface temperatures. This conversion is based on $q/V_h = j^2\rho$ and $\phi = (q/V_h)\ x$, whence $\phi = j^2\rho x$. Since current density and wall thickness were constant with length, the resistivity ratio alone was sufficient for correction of average ϕ to exit ϕ.

The experimental exit burnout fluxes for tests 1 through 7 were compared with values calculated from eight potentially applicable burnout correlations, with the results shown in Table 5.

The correlation equations, along with the ranges of experimental variables on which they are based, are outlined in Table 6. The simple

Table 5. Comparison of Experimental and Calculated Burnout Fluxes

Correlation	Reference	Error[a] (%)	
		Average	Maximum
Jacobs and Merrill	15	47.9	71.6
Hoe and Senghaus	16	37.8	74.0
Bernath	12	26.8	46.5
Buchberg	17	26.1	37.8
Griffith	18	22.8	37.9
Menegus	19	14.8	42.7
McGill and Sibbitt	20	14.3	47.3
Zenkevich and Subbotin	21	14.8	30.6

[a]Calculated minus experimental, divided by experimental, times 100.

Table 6. Boiling Burnout Correlations with Which HFIR Experimental Burnout Data Were Compared

Eq. No.	Proponents	Correlation[a]	Variable Ranges	Reference
2	Jacobs and Merrill	$\phi_{bo} = \psi\ (t_{b_1}, L_h, D_i, P, G)$, see footnote b	t_{b_1} = 72–644°F L_h = 6.0–27.4 in. D_i = 0.075–0.306 in. P = 34–187 atm G = 0.17×10^6–7.79×10^6 lb/hr·ft^2	15
3	Hoe and Senghaus	$\phi_{bo} = 1590\ G^{0.443}\ \Delta t_{sub}^{0.108}$	Δt_{sub} = 1–60°F P = 136 atm G = 0.2×10^6–8.0×10^6 lb/hr·ft^2	16
4	Bernath[c]	$\phi_{bo} = \left[19{,}600\left(\frac{D_e}{D_e + \frac{D_h}{\pi}}\right) + \frac{80.4\ V}{D_e^{0.6}}\right] \times \left[102.6 \ln P - 97.6\left(\frac{P}{P+15}\right) - \frac{V}{2.22} + 32 - (t_b)_{bo}\right]$	D_e < 1.2 in. Δt_{sub} = 0–228°F P = 0.3–204 atm V = 0.3–156.2 fps	12
5	Buchberg	$\phi_{bo} = 520\ G^{0.5}\ \Delta t_{sub}^{0.20}$	D_i = 0.226 in. Δt_{sub} = 3–160°F P = 17–204 atm V = 5–30 fps	17
6	Griffith[c]	$\phi_{bo} = \psi\ (V, \Delta t_{sub}, D, g, H_v, H_b, L_v, \rho_v, \rho_l, \mu_l, k_l, C_{pl})$, see footnote b	Δt_{sub} = 0–200°F x_e = 0–70% P = 1–204 atm V = 0–110 fps	18
7	Menegus[d]	$\phi_{bo} = \psi\ (V, \Delta t_{sub}, D_e, \alpha, \beta_o, \beta_1, \gamma_o, \gamma_1, \delta_1)$, see footnote b	D_e = 0.14–21.2 in. Δt_{sub} = 0–263°F P = 1–150 atm V = 0–54 fps	19
8	McGill and Sibbitt	$\phi_{bo} = 530\ G^{0.5}\ \Delta t_{sub}^{0.28}$	D_i = 0.143 in. t_{b_1} = 85–650°F P = 17–204 atm V = 0.6–40 fps	20
9	Zenkevich and Subbotin	$\phi_{bo} = 396\ G^{0.5}\ \Delta t_{sub}^{0.33}\left(\frac{t_l - t_v}{\rho_l}\right)^{1.8}$	D_e = 0.16–0.47 in. L_h = 7.3–63 in. Δt_{sub} > 13°F P = 102–210 atm G > 0.2×10^6 lb/hr·ft^2	21, 22

[a] Units of variables are as given in the Notation section of this report.

[b] The complete expression is too lengthy to reproduce here.

[c] Also applicable to fluids other than water.

[d] Each of the numerical coefficients (α, β_o, β_1, γ_o, γ_1, and δ_1) varies with pressure.

Zenkevich-Subbotin correlation, Eq. (9), is in good over-all agreement with the data, gives the smallest maximum error, and, in the authors' estimation, can probably be extrapolated with greater confidence than such arbitrarily statistical correlations as those of Jacobs and Merrill[15] and of Menegus.[19] For HFIR design, it was accordingly recommended that the Zenkevich-Subbotin correlation be used with a burnout uncertainty factor of 1.3, that is,

$$(\phi_{bo})_{min} = 305\ G^{0.5}\ \Delta t_{sub}^{0.33} \left(\frac{\rho_l - \rho_v}{\rho_l} \right)^{1.8} . \qquad (10)$$

The 1.3 uncertainty factor is based on the maximum scatter of both the present data and the Soviet data (~870 points). Equation (10) is applicable when $\Delta t_{sub} > 18°F$, $G > 0.2 \times 10^6$ lb/hr·ft^2, and at moderate or high pressures, say $P > 600$ psia (a discussion of the pressure effect follows). The dimensionless density group should be evaluated at the saturation temperature corresponding to system pressure, and the water velocity, temperature, and pressure at the burnout location.

Although Eq. (9) fits the present data, specific to the HFIR geometry, within 15% (average) and 31% (maximum) and the original Soviet data[21,22] for $1500 < P < 3085$ psia within ~10% (average) and 30% (maximum), the correlation was further tested with all other readily available burnout data in order to determine the agreement at lower pressures. The burnout data compiled by Menegus[19] and by Bernath[12] in the development of their correlations were used for the comparison. Tests for which G was $<0.2 \times 10^6$ lb/hr·ft^2 and/or $\Delta t_{sub} < 18°F$ were excluded. The result of the comparison is shown in Fig. 15 as percentage prediction error versus pressure level. For the 105 points taken from Menegus,[19] the average and maximum errors were 66.8% and 355.6%, respectively; the corresponding errors for the 91 points taken from Bernath[12] were 35.7% and 343.0%. The over-all agreement appears best in the range $600 < P < 2200$ psia. The reason for the increasingly poor agreement as the pressure decreases from ~600 to 14 psia is uncertain; it may be caused by an alteration in the mechanism of

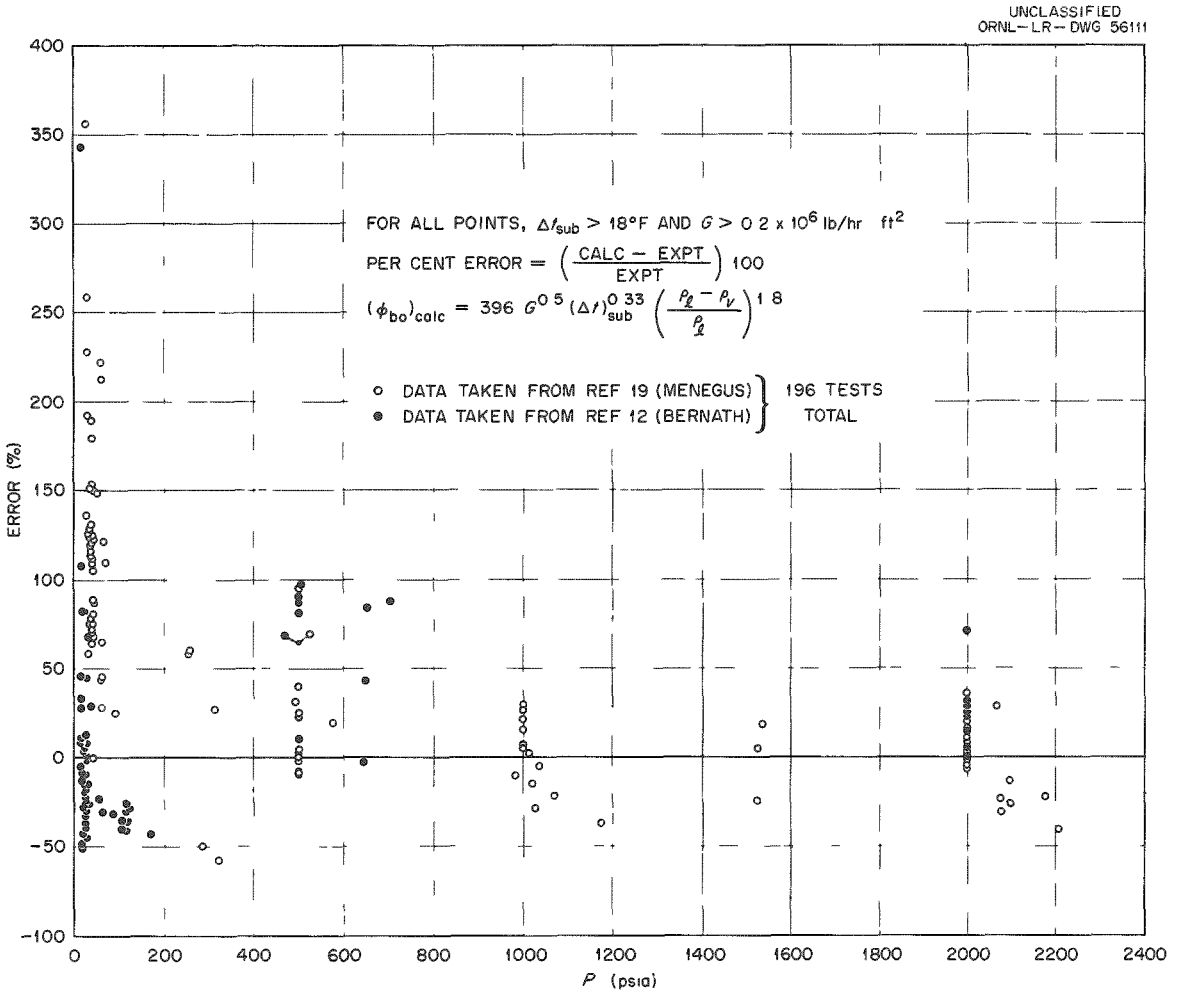

Fig. 15. Variation of Prediction Error with Pressure Level for Zenkevich-Subbotin Burnout Correlation.

the boiling process, by a greater range of experimental inaccuracies arising from the large number of investigators who have worked in the low-pressure region, by a simple failure of the correlation when extended to low pressures, or to the large hydraulic instabilities which characterize certain low-pressure equipment arrangements.[14] The inapplicability of Eq. (9), and of a more generalized dimensionless correlation developed by Zenkevich,[22,23] has been noted by Subbotin for burnout at atmospheric pressure[24] and by Zenkevich for burnout in the range $220 < P < 514$ psia.[23] Evidence contrary to such a trend of large errors at low pressures is given in Appendix I, where the high-velocity straight-flow burnout data for the 22 tests reported in ref. 5, taken at pressures of 10 to 74 psia,

are shown to be predicted reasonably well by the Zenkevich-Subbotin correlation (average and maximum errors of 22% and 70%).

The water used in tests 1 through 3 was not demineralized, and it left scaly surface deposits composed principally of calcium and magnesium salts. The interior surface roughness after burnout was as large as 250 μin. rms in these tests, but the use of demineralized water in tests 4 through 11 reduced the maximum after-test surface roughness to 75 μin. rms. The burnout heat flux did not appear to be significantly influenced by the surface roughness, a result in accord with the conclusions of a memorandum[25] which indicated that surface microroughness (consisting of elements smaller than bubble diameters which do not alter the effective heat-transfer area) does not influence the peak ϕ. It appears, however, that certain arrangements of macroroughness elements — lateral grooves, for example, as discussed in ref. 26 — can enhance burnout fluxes, possibly without a proportionate increase in pumping power.

Burnout safety factors — that is, ratios of minimum probable burnout heat fluxes to maximum operating heat fluxes — were calculated[27] for the HFIR design as it existed in January 1960. The burnout factor was ~2.7 for the case of burnout attainment by power-level increase (which decreases Δt_{sub} and increases ϕ simultaneously), and ~3.6 for the case of a "hot patch" at the core exit — that is, a localized increased heat input which does not significantly affect the subcooling of the coolant at the burnout location. The reactor burnout margins are now somewhat different because of slight changes in core specifications.

Supplementary comparisons between the high-velocity axial-tube-flow burnout data of ref. 5 and four burnout correlations were made with the results outlined in Table 9 in Appendix I.

Present Investigation, Channels with Spacers. In order to minimize heat generation in the longitudinal spacers, they were made from light-wall stainless steel tubing. The spacer dimensions are given in Table 1, and the results of the burnout tests in Table 4. Five test sections with solid spacer strips of square cross section (50 × 50 mils) were partially fabricated but were not tested when it was decided that spacers would not be needed initially.

The experimental burnout fluxes were compared with the same eight correlations with which the empty-channel data were tested (Table 6), and the results are given in Table 7. The predictions of the Zenkevich-Subbotin correlation are in error by only an additional per cent for the spacer tests, Griffith's and Buchberg's correlations show a large improvement relative to the empty-channel data, and the remaining methods are all in poorer agreement than with the empty-channel data.

Table 7. Comparison of Experimental and Calculated Burnout Fluxes

Correlation	Reference	Error[a] (%)	
		Average	Maximum
Hoe and Senghaus	16	77.2	95.7
Bernath	12	76.6	105.9
Jacobs and Merrill	15	69.3	79.0
Menegus	19	59.5	88.3
McGill and Sibbitt	20	31.6	49.8
Zenkevich and Subbotin	21	15.7	31.7
Griffith	18	13.5	17.2
Buchberg	17	9.8	16.6

[a]Only the correlations of Griffith and of Jacobs and Merrill are applicable to test No. 11 (bulk boiling); the other correlations were applied only to tests 8 through 10.

As indicated in more detail in a following section dealing with heat-transfer coefficients, a simple extended-surface analysis (with h assumed as 10^4) indicates that an aluminum spacer strip attached to adjacent aluminum heated plates bounding a 50-mil flow gap would act as a cooling fin, if less than 39 mils wide, and as an insulating strip, if more than 39 mils wide. The "critical" width is reduced to ~6 mils if the strip is solid and made of stainless steel. Since the spacer used was a tube with a 6-mil-wall thickness, some insulating effect was present.

Aside from the insulating tendency of the strip, the burnout heat flux is decreased by strip insertion if G, t_{b_1}, and P are fixed, since the reduced flow area gives, for the same G, a lower total weight flow rate, which corresponds to a greater coolant temperature rise and therefore smaller exit subcooling for a given ϕ. This decrease of ϕ_{bo} resulting from a smaller exit subcooling will appear when empty-channel and spacer data are compared, but will not show up in the comparisons with correlation equations, since in such comparisons the experimental values of G, Δt_{sub}, etc., were used.

One other (more extensive) study of the effect of spacers on burnout was made at the Savannah River Laboratory,[28] where full-length aluminum and silicone-plastic spacer ribs were fixed in rectangular channels (heated from one side only) during a 20-test series with water at low pressure. The results were approximately correlated by the equation

$$-\Delta\phi_{bo} \approx \frac{2400}{e^{50g_s}} \frac{x'}{\sqrt{kx}} , \qquad (11)$$

where

$-\Delta\phi_{bo}$ = percentage reduction in ϕ_{bo},
g_s = rib-to-heated surface clearance, in.,
x' = half-width of rib tip, ft,
x = heated-wall thickness, ft,
k = thermal conductivity of heated surface, Btu/hr·ft·°F.

Equation (11) applies when the wall is cooled from one side only; for cooling both sides with opposed ribs, $-\Delta\phi_{bo} \approx 0.7$ of Eq. (11), and for cooling both sides with unopposed ribs, $-\Delta\phi_{bo} \approx 0.5$ of Eq. (11).

If applied to the HFIR core ($g_s = 0$, $x' = 0.00208$ ft, $x = 0.00416$ ft, and $k = 123$ Btu/hr·ft·°F), Eq. (11) indicates a 4.9% decrease in ϕ_{bo} if the spacers are opposed. If applied to the average experimental conditions for tests 8 through 11 of Table 4 ($g_s = 0.0035$ in., $x' = 0.00238$ ft, $x = 0.003$ ft, and $k = 10$ Btu/hr·ft·°F), Eq. (11) gives a burnout heat flux

reduction of 27.7%. Comparisons of tests 8, 9, and 11 with test 2, and of test 10 with test 3, at constant corrected values of G, P, and Δt_{sub}, indicate that the largest decrements in ϕ_{bo} caused by the presence of the spacers were 25% and 33% (in tests 8 and 9, respectively). Although more tests would be required to reach firm conclusions, it appears that Eq. (11) is suitable for estimation of the maximum decrements of ϕ_{bo} caused by spacers.

Heat-Transfer Coefficients

Preliminary Tests. Early determinations of average heat-transfer coefficients for the nonboiling regime (15 tests) over the Reynolds number range 2.8×10^4 to 1.05×10^5 were made with the nickel test sections (tests 1 through 3 of Table 3 and 4). The results differed from the average data of Levy[2] by a factor of 0.34 to 2.16 because of several complicating factors which were essentially eliminated in the successive tests with aluminum test sections – namely, use of untreated water as coolant, wall temperature drops large in relation to the over-all temperature drop, and what appeared to be significant eddy-current heating in the steel test-section back-up plates.

After axial sectioning of the test sections following burnout, a visual examination of the inner surfaces revealed the presence of white and gray-tan surface deposits. Subsequent semiquantitative spectrographic and chemical analyses indicated that the corrosion deposits were composed principally of calcium and magnesium salts, along with some iron and silicon. The thickness of the oxidation product was determined by electrolytic defilming in boric acid and in chromic-phosphoric acid solutions to be ~0.5 to 2.0 mils for tests 1 through 3. Microscopic examination after defilming revealed numerous small pits, some as deep as 10 mils. Since the thermal conductivity of the surface deposits is known[62] to be ~1 Btu/hr·ft·°F, the thermal resistance of small thicknesses of such deposits is large and tends to obscure the water-film temperature drop used in calculations of heat-transfer coefficients. Similar tests on the surface deposits generated in tests 5 and 7 (after the change to all stainless piping, aluminum test sections, and distilled water) indicated thicknesses

of only 0.03 to 0.09 mils, which were too small to significantly affect the derived heat-transfer coefficients. The wall temperature drop was greatly decreased by changing from 60-mil-thick nickel to 35-mil-thick type 1100 aluminum after test 3. The eddy-current heating was effectively eliminated after test 2 by changing to stainless steel back-up plates electrically isolated along a bolt row. Since heat-transfer coefficients for water at high Reynolds numbers are quite large ($3120 < h_x < 38{,}200$ Btu/hr·ft^2·°F in this study), their reliable measurement requires much care and regard for such factors.

As a result of these considerations, only the heat-transfer coefficients derived from the aluminum test sections are reported here. All tests were conducted as quickly as possible in order to minimize Al_2O_3 formation, and in general lasted no longer than 1 hr.

Results Without Spacers. The heat flux was based on the coolant heat absorption rate and the internal heated surface area. The temperature drop through the wall did not exceed 40°F during coefficient determinations with the aluminum test sections and was calculated according to $\Delta t_w = \phi x/2k$. This simplest solution to the conduction equation for the case of volumetric heat generation was checked with the numerical zone-type solution of Stein and Gutstein,[29] which includes the influence of the thermal dependencies of the thermal and electrical conductivities, and was found to involve an error in $\Delta t_w < 5\%$. Electrical resistivity data were taken from ref. 30 and values of thermal conductivity for pure aluminum from the International Critical Tables.[31]

For each of the tests, a plot of the length variation of the pertinent temperatures was made, as illustrated by Fig. 16 for steady state No. 8 of test No. 7. Except for the scatter of the measured wall temperatures, which is larger than in nearly any of the 30 other experimental steady-state runs, Fig. 16 is typical of the length variation graphs prepared. Wall saturation temperatures were taken from steam tables to correspond to the measured terminal static pressures. The coolant bulk temperature was assumed to vary linearly with x, and a zone calculation indicated that the error incurred by this assumption was negligible. Local heat-transfer coefficients were computed at each axial temperature-measurement

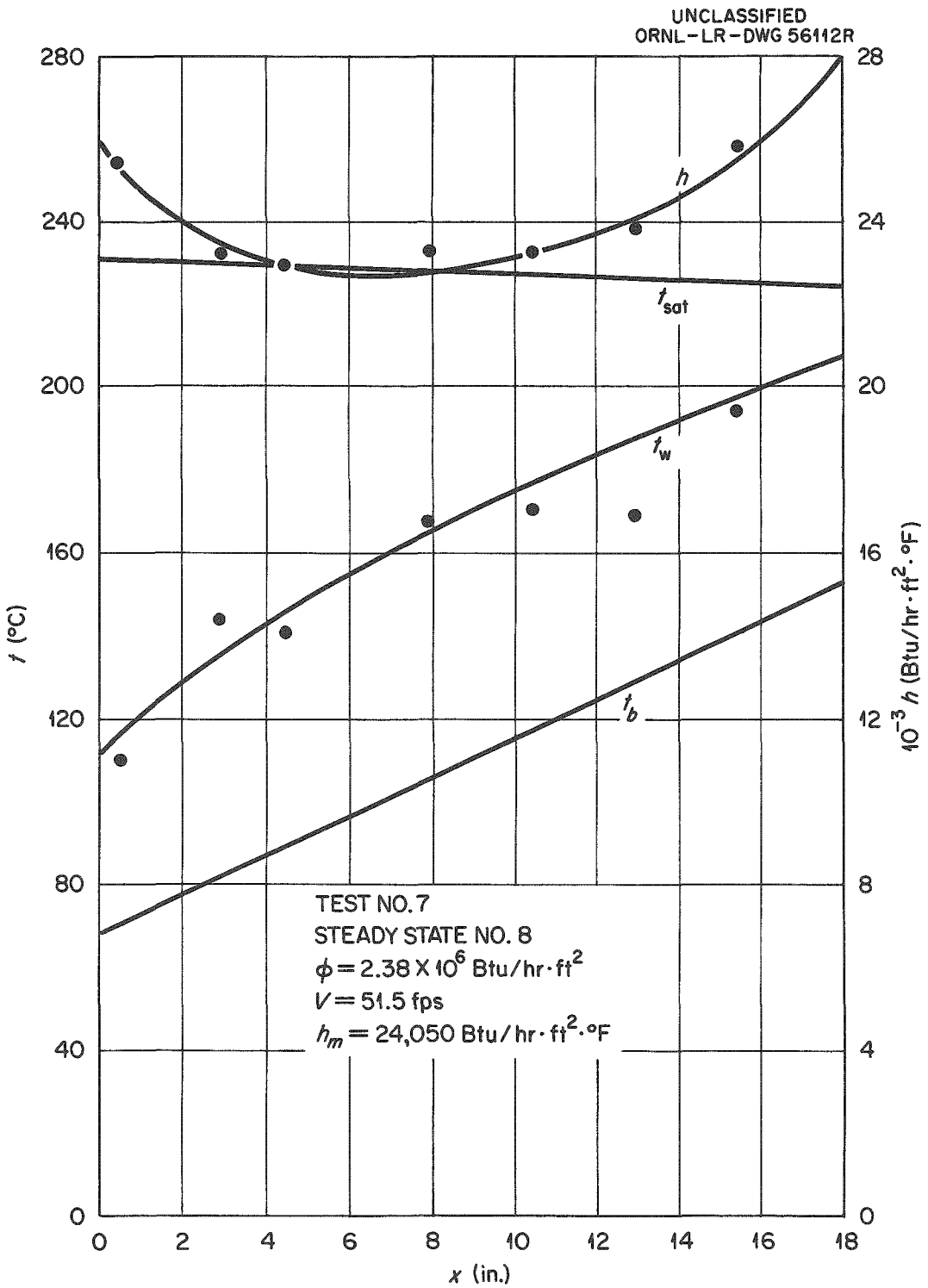

Fig. 16. Typical Plot of Variation of Pertinent Temperatures and of Heat-Transfer Coefficient with Heated Length.

station with

$$h_x \equiv \frac{\phi_x}{(t_w - t_b)_x} \quad ,$$

and the resulting curve was graphically integrated to obtain an average h for the test section. All measured temperatures were used in these calculations, including those at the lateral locations. Measured h values can vary with x for three reasons: development or growth of the boundary layer, laminar-turbulent boundary-layer transition, and variation of coolant physical properties with temperature. In Fig. 16, the initial decrease of h because of entrance-region thermal boundary-layer development, as well as the subsequent increase of h associated with a favorable change of physical properties, may be noted. The initial sharp dip in curves of h versus x associated with coincidence of thermal and hydrodynamic starting sections[32] was sometimes, but not always, observed.

The 31 derived average heat-transfer coefficients are compared in Fig. 17 with the Sieder-Tate equation,[3]

$$(Nu)_{bm} = 0.027\ (Re)_b^{0.8}\ (Pr)_b^{1/3}\ (\mu_b/\mu_w)^{0.14} \quad , \qquad (12)$$

and with the mean and minimum curves through the data collection of Levy and co-workers.[2] The data, which cover the range $1.14 \times 10^4 < (Re)_{bm} < 1.67 \times 10^5$, are obviously in better agreement with the usual formulation than with the lower-than-normal data reported by Levy. None of the present data fall more than 26% below the line representing Eq. (12), whereas the mean data of ref. 2 are 32 to 57% lower over the Reynolds number range 2×10^4 to 1×10^5. Of the new data plotted in Fig. 17, only three points deviate negatively by more than 10% from Eq. (12), and it appears that

$$(Nu)_{bm} = 0.024\ (Re)_b^{0.8}\ (Pr)_b^{1/3}\ (\mu_b/\mu_w)^{0.14} \qquad (13)$$

is a reasonably conservative design relation.

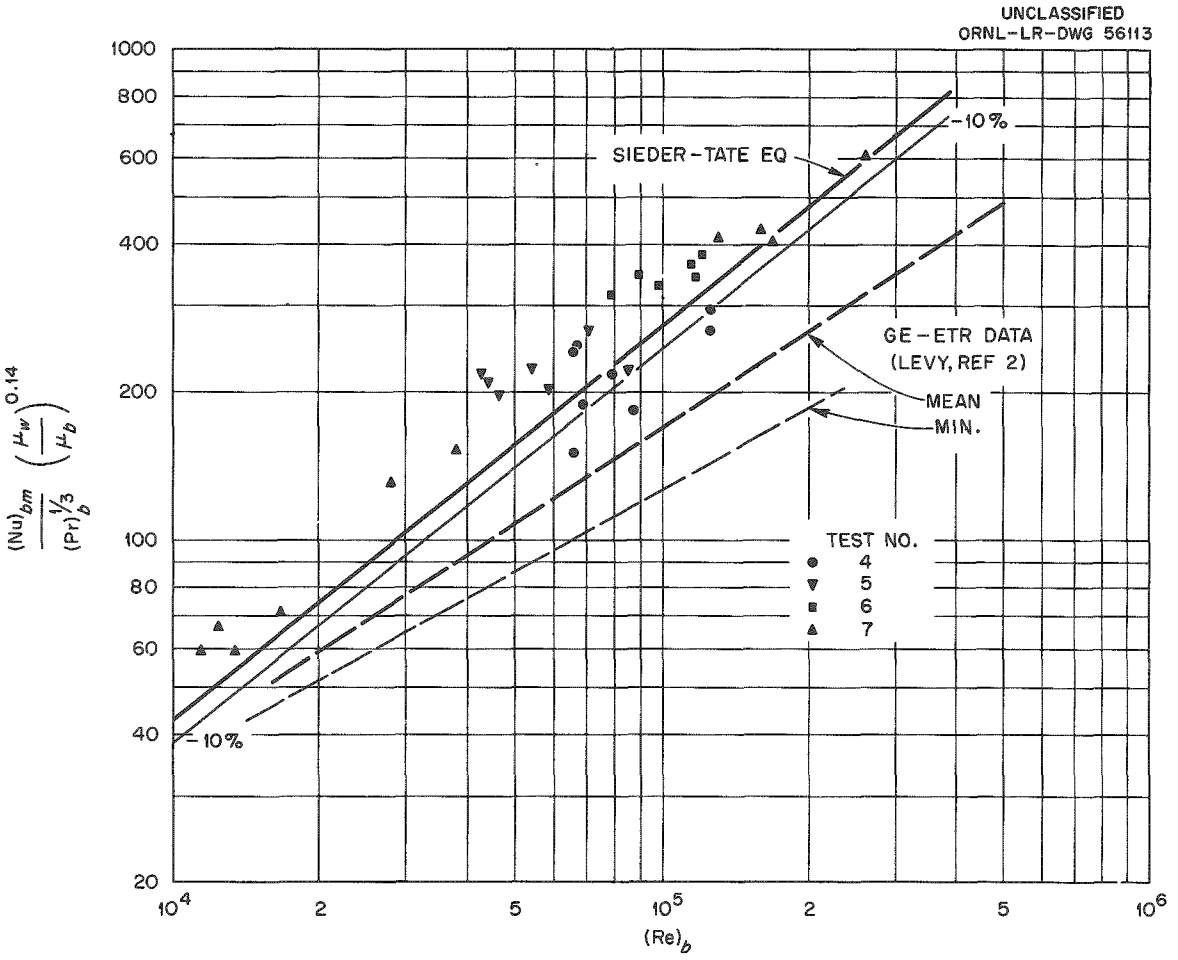

Fig. 17. Average Heat-Transfer Coefficients for Thin Rectangular Channels Compared with the Sieder-Tate Correlation and with the Data of Levy.

Slightly better correlation of the same data was obtained when it was reduced according to the Hausen equation:

$$(Nu)_{bm} = 0.116 \left[(Re)_b^{2/3} - 125\right] (Pr)_b^{1/3} \left[1 + \left(\frac{D_e}{L_h}\right)^{2/3}\right] \left(\frac{\mu_b}{\mu_w}\right)^{0.14} , \quad (14)$$

as shown in Fig. 18. The Hausen correlation[32] is applicable to both the transition and turbulent flow regimes and supposedly takes into account conditions in the thermal intake region. Only two points fall below Eq. (14) when it is reduced by 6%, which is given by

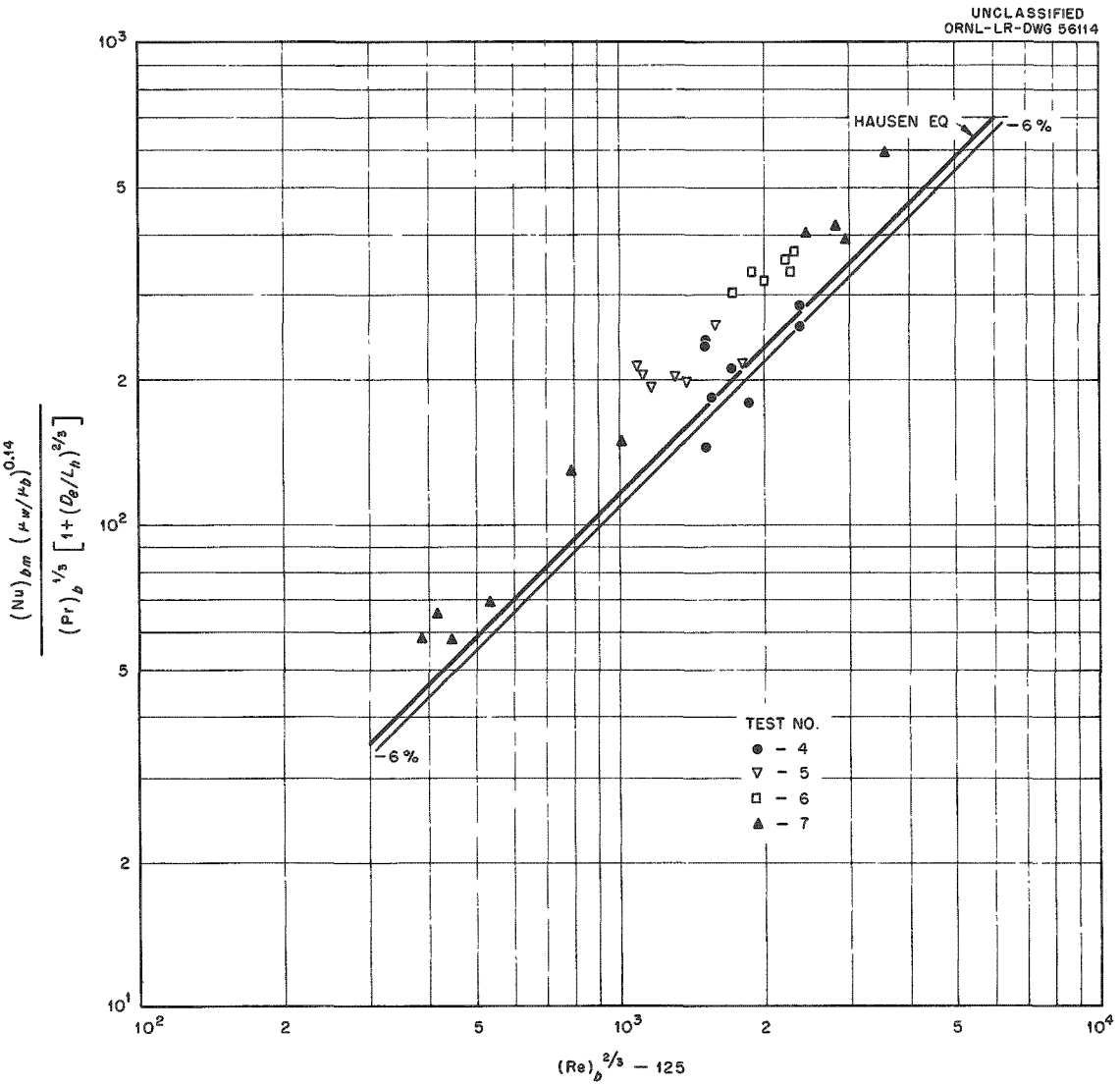

Fig. 18. Average Heat-Transfer Coefficients for Thin Rectangular Channels Compared with the Correlation of Hausen.

$$(Nu)_{bm} = 0.109\left[(Re)_b^{2/3} - 125\right](Pr)_b^{1/3}\left[1 + \left(\frac{D_e}{L_h}\right)^{2/3}\right]\left(\frac{\mu_b}{\mu_w}\right)^{0.14}, \qquad (15)$$

and which was recommended as the design correlation for average h under HFIR conditions.

Some 240 local heat-transfer coefficients were derived from the measurements. Local heat-transfer coefficients exhibit more scatter than mean values because of necessary reliance on point measurements and the

absence of averaging over the whole test section, which tends to suppress the deviation of extreme values. The conditions that $\Delta t_f \geq 15°C$ and $x/D_e \geq 30$ were imposed on the final data treatment. The film temperature-drop condition was necessary in order to exclude tests where Δt_f was so small that only minor thermocouple and other experimental inaccuracies could introduce very large errors in the derived h values. The x/D_e condition limits the data considered to those obtained at measurement locations relatively free from particular entrance-condition influences. In the presently proposed HFIR core, the fuel plates will extend 3 in. at top and bottom beyond the active (fueled) length, so that an x/D_e of 30 will exist as a hydrodynamic intake region.

The local h predicted by the Hausen equation may be obtained by differentiation of the correlation for h_m, since, by definition,

$$h_m = \frac{\int_0^{x/D} h_{x/D}\, d\left(\frac{x}{D}\right)}{\frac{x}{D}} \tag{16}$$

With reference to Eq. (14), let

$$K = 0.116\left(\frac{k}{D}\right)\left(\frac{\mu_b}{\mu_w}\right)^{0.14} (Pr)_b^{1/3}\left[(Re)_b^{2/3} - 125\right] \tag{17}$$

so that

$$h_m = K\left[1 + \left(\frac{D}{x}\right)^{2/3}\right] \tag{18}$$

From Eq. (16):

$$h_{x/D} = \frac{d\left[h_m\left(\frac{x}{D}\right)\right]}{d\left(\frac{x}{D}\right)} = \frac{d\left\{K\left[1 + \left(\frac{D}{x}\right)^{2/3}\right]\left(\frac{x}{D}\right)\right\}}{d\left(\frac{x}{D}\right)}\,, \tag{19}$$

and

$$h_{x/D} = \frac{d\left[K\left(\frac{x}{D}\right) + K\left(\frac{x}{D}\right)^{1/3}\right]}{d\left(\frac{x}{D}\right)} = K\left[1 + \frac{1}{3}\left(\frac{D}{x}\right)^{2/3}\right] \qquad (20)$$

with the result that

$$(Nu)_x = 0.116\left[(Re)_{bx}^{2/3} - 125\right](Pr)_{bx}^{1/3}\left[1 + \frac{1}{3}\left(\frac{D}{x}\right)^{2/3}\right]\left(\frac{\mu_b}{\mu_w}\right)_x^{0.14} . \qquad (21)$$

The data of this study are shown plotted according to Eq. (21) for all the data meeting the criteria noted above (177 points) as Fig. 19, and for test No. 7 only (56 points) as Fig. 20. In Fig. 19, 92% of the data fall on or above the line representing Eq. (21), 95% above Eq. (21) when reduced by 10%, and 99% when reduced by 25%. It appears that a 10% reduction, corresponding to

$$(Nu)_{bx} = 0.105\left[(Re)_{bx}^{2/3} - 125\right](Pr)_{bx}^{1/3}\left[1 + \frac{1}{3}\left(\frac{D_e}{x}\right)^{2/3}\right]\left(\frac{\mu_b}{\mu_w}\right)_x^{0.14} , \qquad (22)$$

represents a reasonable design recommendation.

Two other studies recently reported confirm the range of heat-transfer coefficients reported here. Stanley and Conway[33] determined local h values for flow of low-pressure air at $70 < t_b < 500°F$ through both 0.44-in.-i.d. type 310 stainless steel tubes and through Nichrome rectangular channels measuring 1.5 in. × 0.125 in. × 12 in. long. For the range $10^4 < (Re)_f (T_b/T_f) < 3 \times 10^4$, the best line through the rectangular-channel data is 6 to 15% higher than the best tube-data line. Heineman[34] cooled both 0.333-in.-i.d. tubular and 1.25-in. × 0.047-in. rectangular test sections with superheated steam over the following ranges of the variables:

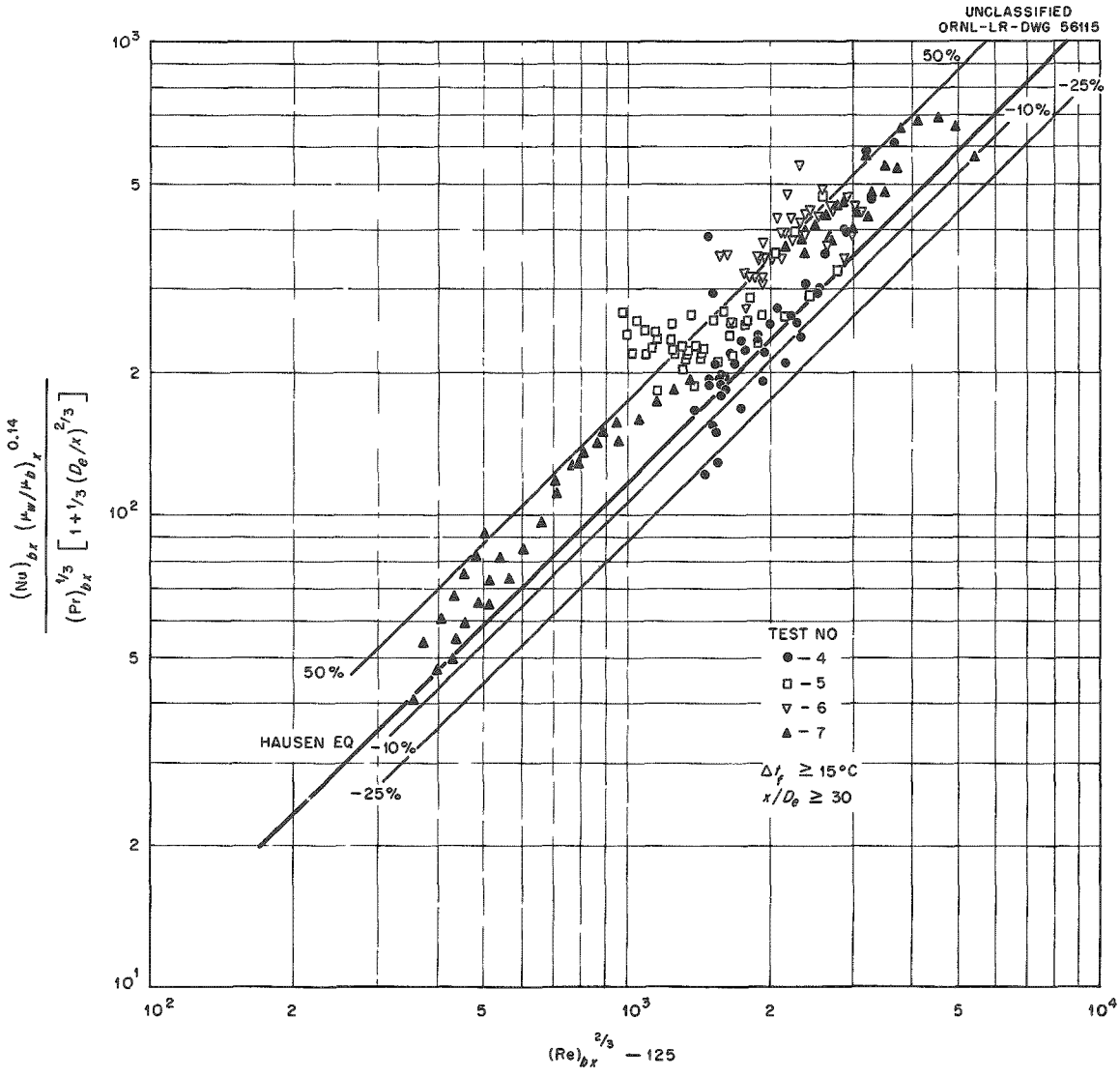

Fig. 19. Local Heat-Transfer Coefficients for Thin Rectangular Channels Compared with the Correlation of Hausen.

$300 < P < 1500$ psia	$23 \times 10^3 < \phi < 287 \times 10^3$ Btu/hr·ft^2
$470 < t_b < 900°F$	$25 \times 10^3 < Re < 370 \times 10^3$
$520 < t_w < 1290°F$	$30 < \Delta t_f < 550°F$

He concluded that there is no observable difference between the rectangular-channel data and the round-channel correlation in the L_h/D_e range from 60 to 121, and that there is no reason to expect any important differences at larger values of L_h/D_e. Heineman also noted that the vena contracta

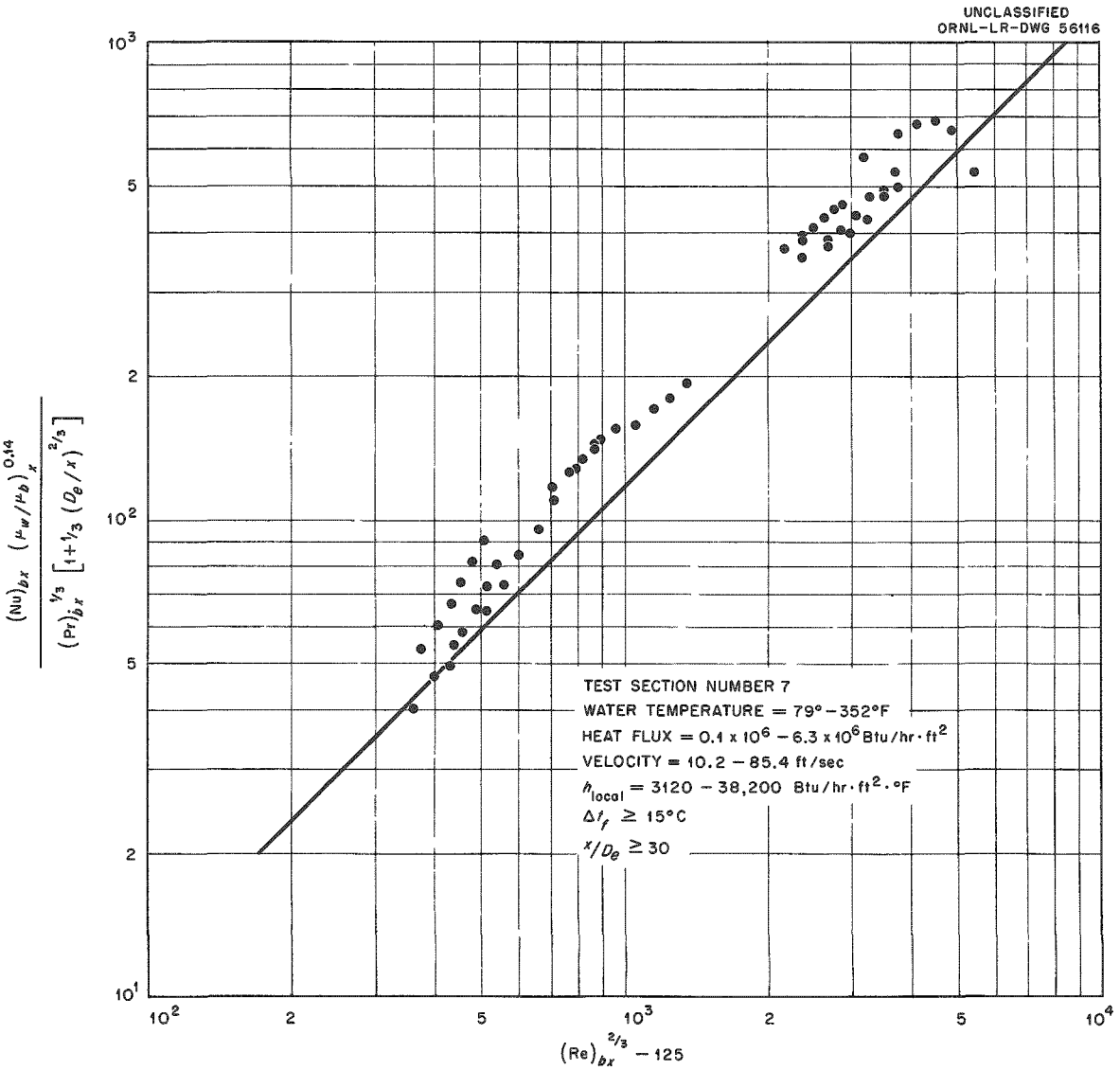

Fig. 20. Local Heat-Transfer Coefficients for Thin Rectangular Channels Compared with the Correlation of Hausen.

caused by the sharp-edged entrance condition of his test section influenced h (increasing it) up to an L_h/D_e of ~60. The data of the present study and of refs. 33 and 34 appear to lend confidence to the standard heat-transfer-coefficient correlations when applied to the turbulent flow of fluids through thin rectangular channels and to strongly suggest the invalidity of the data of Levy et al.[2]

Heineman[34] also measured a few wall-temperature profiles across the width of his test section and found that the slight increases in temperature

measured at points one-sixth of the width from the edge caused a maximum change in the centerline coefficient of ~5%. Fifteen similar comparisons of the present data from tests 4 through 7 were made for nominal HFIR steady-state conditions – that is, $\phi = 0.8 \times 10^6$ to 1.4×10^6 Btu/hr·ft^2 and $(\Delta t_f)_m \approx 33°C$ – and it was found that the average lateral variation of h was 10.9%. Most of the variations, which tended generally to increase with heated length, were negative. The studies of Heineman were made with much larger average values of Δt_f than were measured in the present tests, and the smaller lateral variations of h reported by him are probably more characteristic of turbulent flow through uniform-flux rectangular channels.

Results with Spacers. If a full-length spacing strip between parallel flat plates is assumed to be oriented parallel to the flow direction with negligible contact resistances between the spacer and heated walls, it is possible to make a simple analysis[35,36] to determine the approximate strip width above which the strip acts as an insulator and below which it acts as a cooling fin. If W_s is the width of a rectangular plane spacer (see Table 1), let $W_s/2 = b$ = one-half spacer thickness. If g is the flow gap, then

$$\frac{q_{fin}}{q_{no\ fin}} = \frac{A_{fin\ surface}}{A_{fin\ base}}\,\eta \tag{23}$$

and for this case,

$$\eta = \frac{\tanh mg}{mg}\ , \tag{24}$$

where $m = \sqrt{h/kb}$. From Eqs. (23) and (24),

$$\frac{q_{fin}}{q_{no\ fin}} = \frac{(g/2)(2)(1)}{(2b)(1)}\,\frac{\tanh mg}{mg} = \frac{g}{2b}\,\frac{\tanh mg}{mg} \tag{25}$$

For the condition $q_{fin} = q_{no\ fin}$, the criterion is therefore:

$$2b = \frac{\tanh mg}{m} \quad . \tag{26}$$

For HFIR conditions — that is, $g = 0.050$ in., $h \approx 10^4$ Btu/hr·ft²·°F, and $k = 120$ Btu/hr·ft·°F — Eq. (26) is satisfied by $2b = 0.039$ in. For the conditions of the spacer tests (tests 8 through 11 of Tables 3 and 4) — that is, $g = 0.057$ in. (av), $h \approx 10^4$, and $k = 10$ — the equation is satisfied by $2b$ = spacer width = 0.006 in. The stainless steel spacers used in the tests were tubular (6-mil wall) and were not cooled internally; in the sense of this analysis they should act approximately as miniature I-beams with a 12-mil web thickness and ~30-mil flange width (the width of the flattened portion of the tube adjoining the aluminum wall). The outside surface temperatures over the spacers would accordingly be expected to be higher than those at the sides of the spacer. This proved to be the case, as shown in Table 8. The data variability are due partially to probable spacer vibration and to variations in the axial spacer-to-wall clearance (given in Table 1). The reason for the unusually large temperature increases measured during test 9 is not known. The maximum increases occurred within the initial 5 in. of the heated length in tests 8 and 9, in the downstream half in test 10, and at $\sim L_h/2$ in test 11. The use of 50 × 50-mil aluminum spacers in an HFIR core should result in smaller temperature increases than those given above; the estimated maximum is 6°C.

Table 8. Temperature Data for Tests 8 Through 11

Test No.	Minimum t Increase at $\phi = 1.5 \times 10^6$ (°C)	Maximum t Increase at $\phi = 1.5 \times 10^6$ (°C)	Over-all Maximum t Increase (°C)	At ϕ (Btu/hr·ft²)
8	1	9	10	1.90×10^6
9	7	20	22	2.05×10^6
10	0	7	10	3.03×10^6
11	0	8	9	3.18×10^6

An experimental and theoretical study of the effect of spacers on plate temperature distributions was conducted at Battelle Memorial Institute[37-40] in connection with a proposed nuclear reactor cooled by supercritical water. Discontinuous cylindrical spacers were considered, oriented either parallel to the flow direction or normal to the fuel plate. It was found, in general, that the use of such discontinuous spacers resulted in slightly lower maximum surface temperatures than were measured in the absence of spacers. This decrease was attributed in large part to increased stream turbulence caused by flow readjustment at the leading edges of the spacers.

Post-test examination[41] of the inner surface of the test section used in test 9 revealed a narrow band of localized corrosion attack along the portion of the aluminum surface contacted by the spacer tube. The band, ~1/16 in. wide, extended the full length of the test section. The attacked region appeared to be covered by a bulky white corrosion product superimposed over a thinner layer of golden-colored corrosion product. Enlarged views of the sections studied are shown after electrolytic defilming in Fig. 21. The attack resulted in some rippling of the surface and in numerous pits (6.1-mil maximum depth). The observed attack could be attributed[41] to galvanic coupling between the aluminum and stainless steel, to concentration-cell contact corrosion, or to fretting. In any event, it appears that use of unattached spacer strips under high-velocity, high-temperature conditions with aluminum is impractical except for very short-term applications.

Acknowledgments

The authors wish to express their appreciation to J. Lones and D. H. Wallace for their valuable assistance as project technicians, to W. S. Harris of Reactor Projects Division and R. J. Fox of Engineering and Mechanical Division for their suggestions during the early test-section design stages, to C. R. Rickard of the ORNL Research Shops for skillful fabrication of the test sections, to W. C. Colwell of Graphic Arts for preparation of the illustrations, and to Dolores Eden for her conscientious typing of the manuscript.

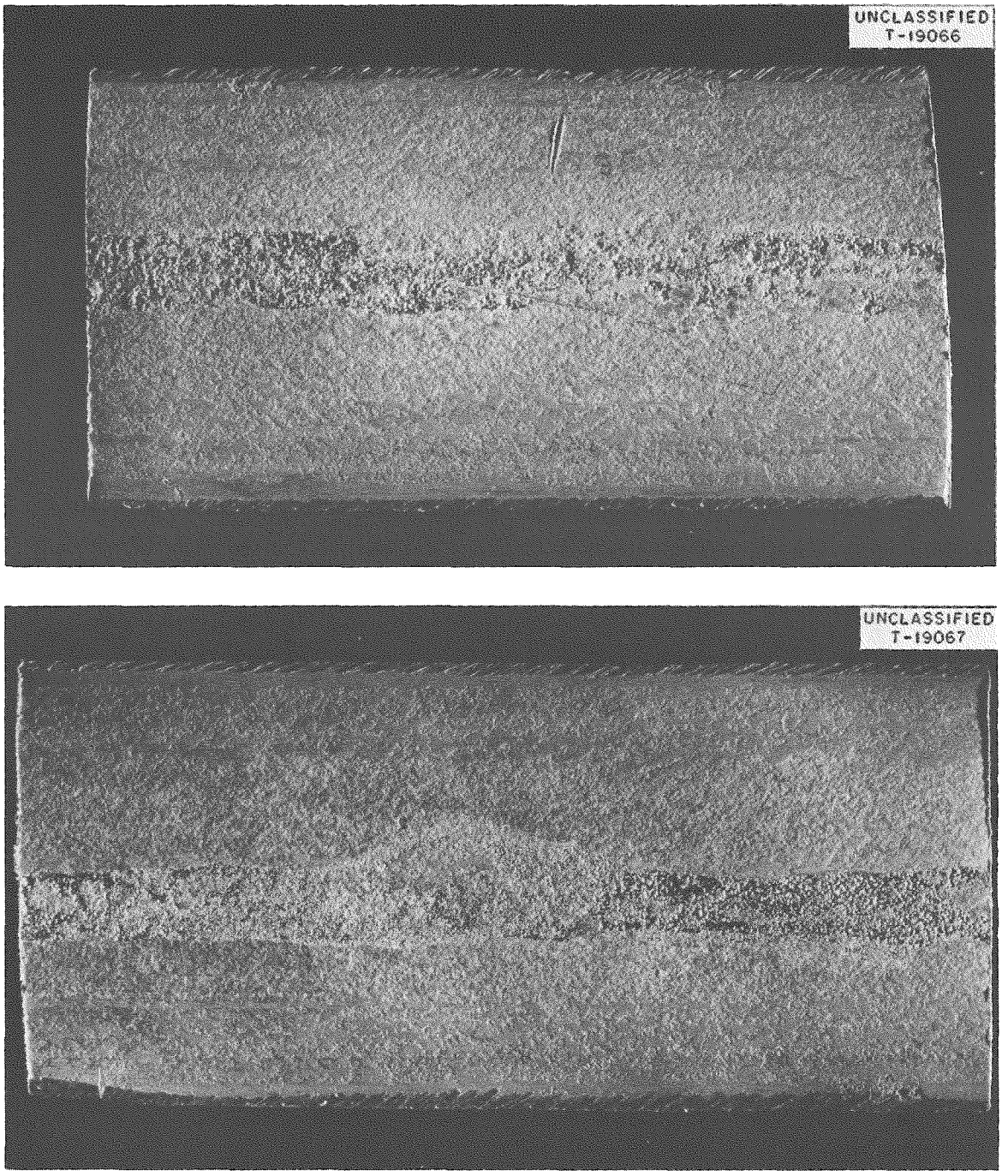

Fig. 21. Two Views Showing Type of Attack Experienced by Type 1100 Aluminum Heat-Flux Specimen on Area Contacted by Stainless Steel Spacer Tube. 5.9X

Notation

(Listed units are used except where otherwise noted)

a_f	net flow area of coolant passage, in.^{2}
A_h	internal heated surface area, ft^2
A_x	cross-sectional metal area, ft^2
b	half spacer width (g + 2x in Fig. 6 only), in.
C_p	constant-pressure specific heat of coolant, Btu/lb·°F
D	diameter of flow passage
D_e	equivalent diameter of flow passage, ft
D_i	inside tube diameter, ft
dt	axial temperature rise of coolant, °F
E	electrical potential across test section, volts
f	friction factor, dimensionless
g	flow gap, in.; acceleration of gravity, 4.18×10^8 ft/hr^2
g_s	clearance between spacer and heated surface, in.
G	coolant mass velocity, lb/hr·ft^2
$\overline{Gr}$	channel-average Grashof number, $D_e^3\rho^2 g\beta(\Delta t)_f/\mu^2$, dimensionless
h	surface heat-transfer coefficient, Btu/hr·ft^2·°F
h_s	height of spacer (see Table 1), in.
H	enthalpy of coolant fluid, Btu/lb
I	electrical current through test section, amp
j	current density in heated metal, I/A_x, amp/ft^2
k	thermal conductivity, Btu/hr·ft^2·°F/ft
$\overline{Ka}$	channel-average von Karman number, 2f Re^2, dimensionless
L	length of test section, ft
L_v	latent heat of vaporization of coolant, Btu/lb
Nu	Nusselt number, hD_e/k, dimensionless
p_h	heated internal perimeter of test section, in.
P	static pressure of coolant, psia
Pr	Prandtl number of coolant, $C_p\mu/k$, dimensionless
q	heat-transfer rate, Btu/hr
R	electrical resistance of test section, ohms
Re	Reynolds number, D_eG/μ, dimensionless

t	temperature, °F
T	absolute temperature, °R
Δt_f	film temperature drop, $(t_w - t_b)$, °F
Δt_{sub}	degree of subcooling of coolant, $(t_{sat} - t_b)$, °F
Δt_w	wall temperature drop, $(t_{wo} - t_{wi})$, °F
V	linear coolant velocity, fps
V_h	heated-wall volume, ft^3
W	coolant weight flow rate, lb/hr
W_s	width of spacer, 2b, in.
x	local axial length (measured from beginning of heated length), ft; thickness of heated wall, ft
x_e	exit vapor quality, wt % steam
β	volumetric coefficient of thermal expansion of coolant, $(°F)^{-1}$
ϵ	average height of surface microroughness elements, ft
η	thermal fin efficiency
μ	dynamic viscosity of coolant, lb/hr·ft
ρ	coolant density, lb/ft^3; electrical resistivity of metal, ohm-ft
ρ_e	electrical resistivity of coolant water, ohm-cm
ϕ	heat flux, q/A_h, $Btu/hr \cdot ft^2$
ψ	indicates functional dependence

Subscripts

a	afterheat
b	bulk (mixed-mean) value
bo	burnout
calc	calculated
f	film; friction
h	heated
i	internal
iso	isothermal
l	of liquid
*l*b	local boiling
m	mean value
max	maximum value
min	minimum value

nb	nonboiling
o	outside
s	of spacer
sat	saturation
v	of vapor
w	at inner surface of heated wall
x	local; cross-sectional
1	at test-section inlet
2	at test-section exit

Literature Cited

1. T. E. Cole, High Flux Isotope Reactor, A General Description, ORNL CF-60-3-33 (Mar. 15, 1960).

2. S. Levy, R. A. Fuller, and R. O. Niemi, "Heat Transfer to Water in Thin Rectangular Channels," J. of Heat Transfer 81, No. 2, 129–43 (1959).

3. E. N. Sieder and G. E. Tate, "Heat Transfer and Pressure Drop of Liquids in Tubes," Ind. Eng. Chem. 28, No. 12, 1429–35 (1936).

4. R. T. Lancet, "The Effect of Surface Roughness on the Convection Heat-Transfer Coefficient for Fully Developed Turbulent Flow in Ducts with Uniform Heat Flux," J. of Heat Transfer 81, No. 2, 168–74 (1959).

5. W. R. Gambill, R. D. Bundy, and R. W. Wansbrough, Heat Transfer, Burnout, and Pressure Drop for Water in Swirl Flow Through Tubes with Internal Twisted Tapes, ORNL-2911 (Mar. 28, 1960).

6. W. H. Esselman et al., Thermal and Hydraulic Experiments for Pressurized Water Reactors, U. S. Geneva Conference Paper, A/Conf. 15/P/453, Figs. 4 and 5 (June 1958).

7. L. F. Moody, "Friction Factors for Pipe Flow," Trans. Am. Soc. Mech. Engrs. 66, 671–84 (1944).

8. W. M. Jacobi et al., "Thermal Design Criteria for Pressurized-Water Reactors," Nucleonics 16, No. 11, 130–4, 199 (1958).

9. R. A. DeBortoli et al., Forced-Convection Heat Transfer Burnout Studies for Water in Rectangular Channels and Round Tubes at Pressures Above 500 psia, WAPD-188 (Oct. 1958).

10. R. H. DeBortoli, Departure from Nucleate Boiling Tests at 2000 psia on Rectangular Channels with a Flux Peak in the Corners, WAPD-AD-TH-519 (June 8, 1959).

11. H. M. Kolm, "Recent Advances in the Design of High-Field dc Solenoid Magnets," J. Appl. Phys. 29, No. 3, 489–91 (1958).

12. L. Bernath, A Theory of Local Boiling Burnout and Its Application to Existing Data, Preprint No. 110, Third National Heat Transfer Conference, ASME-AIChE, Storrs, Conn. (August 1959).

13. N. L. Kafengauz and I. D. Bauarov, "The Effect of the Height of a Flat Aperture on the Transformation of Heat into Water," Teploenergetika, No. 3, 76–78 (1959).

14. W. H. Lowdermilk, C. D. Lanzo, and B. L. Siegel, Investigation of Boiling Burnout and Flow Stability for Water Flowing in Tubes, NACA-TN-4382 (Sept. 1958).

15. R. T. Jacobs and J. A. Merrill, "The Application of Statistical Methods of Analysis for Predicting Burnout Heat Flux," Nuclear Sci. and Eng. 8, No. 6, 480–96 (1960).

16. R. H. Hoe and L. A. Senghaus, "Correlation of Subcooled and Quality Burnout Data for Cylindrical Tubes and Rectangular Ducts," Reactor Heat Transfer Progress No. 12, ed. by J. E. Viscardi, NDA-31 (declassified) (Oct. 30, 1956).

17. H. Buchberg et al., Final Report on Studies in Boiling Heat Transfer, COO-24, University of California (March 1951).

18. P. Griffith, The Correlation of Nucleate Boiling Burnout Data, ASME Preprint No. 57-HT-21, First National Heat Transfer Conference, ASME-AIChE, University Park, Pa. (Aug. 1957).

19. R. L. Menegus, Burnout of Heating Surfaces in Water, AEC R&D Rep. DP-363 (March 1959).

20. H. L. McGill and W. L. Sibbitt, Heat Transfer and Pressure Drop of Water Flowing in a Small Tube, ANL-4603, Part I (Feb. 1951).

21. B. A. Zenkevich and B. I. Subbotin, "Critical Heat Fluxes in Sub-Cooled Water with Forced Circulation," Atomnaya Energiya 3, 149 (1957); English translation in J. Nuclear Energy, Part B: Reactor Technology 1, No. 2, 134–6 (1959).

22. B. A. Zenkevich, "Similarity Criteria for Critical Heat Loading in Forced Liquid Flow," Atomnaya Energiya 4, 74 (1958); English translation in J. Nuclear Energy, Part B: Reactor Technology 1, No. 2, 137–40 (1959).

23. B. A. Zenkevich, "The Generalization of Experimental Data on Critical Heat Fluxes in Forced Convection of Subcooled Water," Atomnaya Energiya 6, 169 (1959); English translation in J. Nuclear Energy, Part B: Reactor Technology 1, No. 2, 130–3 (1959).

24. N. Zuber, Ramo-Wooldridge Corp., private communication to W. R. Gambill, Feb. 24, 1960.

25. W. R. Gambill, Comments on the Effect of Surface Roughness on Burnout Heat Flux, internal memorandum to C. E. Winters, Dec. 3, 1959.

26. W. S. Durant and S. Mirshak, Roughening of Heat Transfer Surfaces as a Method of Increasing the Heat Flux at Burnout, DP-380, Prog. Rep. No. 1 (July 1959).

27. W. R. Gambill and R. D. Bundy, HFIR Burnout Safety Factors, internal memorandum to C. E. Winters, Feb. 24, 1960.

28. S. Mirshak and W. S. Durant, Savannah River Laboratory, private communication to W. R. Gambill, Jan. 29, 1960.

29. R. P. Stein and M. U. Gutstein, Temperature Distribution in Solids with Electrical Heat Generation and Temperature Dependent Properties, Preprint 117, Third National Heat Transfer Conference, ASME-AIChE, Storrs, Conn. (Aug. 9–12, 1959).

30. W. R. Gambill, Electrical Resistivity Data for Heat-Transfer Test-Section Metals, ORNL CF-59-4-89 (Apr. 15, 1959).

31. International Critical Tables, p. 220, Vol. V, McGraw-Hill Book Co., New York, 1929.

32. E. R. G. Eckert and R. M. Drake, Jr., Heat and Mass Transfer, pp. 212–13, McGraw-Hill Book Co., New York, 1959.

33. R. A. Stanley and J. B. Conway, Determination of Local Heat Transfer Coefficients by a Transient Technique, Preprint V-40, Nuclear Eng. and Sci. Conference, Cleveland, Ohio, April 6–9, 1959.

34. J. B. Heineman, An Experimental Investigation of Heat Transfer to Superheated Steam in Round and Rectangular Channels, ANL-6213 (Sept. 1960).

35. J. G. Bartas, "Gas-Side Wall Temperatures in Rib-Backed Liquid-Cooled Combustion Chambers," Jet Propulsion, 784–6 (July 1957).

36. D. Q. Kern, Process Heat Transfer, 1st ed., chap. 16, "Extended Surfaces," pp. 512–62, McGraw-Hill Book Co., New York, 1950.

37. J. W. Chastain et al., Temperature Distributions in a Reactor Fuel Plate, BMI-872 (Sept. 25, 1953).

38. R. F. Redmond et al., Temperature Distributions in a Reactor Fuel Plate. II. Parallel Plates with Longitudinal Cylindrical Spacers, BMI-906 (Mar. 12, 1954).

39. J. K. Long et al., Temperature Distributions in a Reactor Fuel Plate. III. Parallel Plates with Perpendicular Cylindrical Spacers, BMI-907 (Mar. 12, 1954).

40. R. M. Evans and D. C. Martin, Evaluation of Methods of Brazing Aluminum Spacing Fins to Flat-Plate Aluminum-Clad Fuel Elements, BMI-929 (July 23, 1954).

41. J. L. English, Post-Test Examination of Type 1100 Aluminum Heat-Flux Specimen, internal letter to W. R. Gambill, July 12, 1960.

42. S. Mirshak, W. S. Durant, and R. H. Towell, Heat Flux at Burnout, DP-355 (Feb. 1959).

43. P. I. Povarin and S. T. Semenov, "Investigation of the Abrupt Change in Boiling of Water Heated Under the Saturation Temperature at High Flow Rates Through Pipes," Teploenergetika, No. 4, 72–79 (1959).

44. N. Hilvety, Gamma and Beta Heat Generation Rates in the HFIR Core, ORNL CF-60-4-110 (Apr. 29, 1960).

45. W. R. Gambill and R. D. Bundy, originally reported as HFIR Minimum Shut-Down Flow Rate, internal memorandum to C. E. Winters, June 15, 1960.

46. C. F. Bonilla, Nuclear Engineering, chap. 8, "The Flow of Fluids," pp. 322–5, McGraw-Hill Book Co., New York, 1957.

47. W. H. Jens and P. A. Lottes, Analysis of Heat Transfer, Burnout, Pressure Drop, and Density Data for High Pressure Water, ANL-4627 (May 1, 1951).

48. F. T. Binford, W. R. Gambill, and J. F. Wett, Jr., Comments on WTR Fuel Meltdown, ORNL CF-60-5-33, pp. 20–23 (May 9, 1960).

49. E. F. Leib, Trans. Am. Soc. Mech. Engrs. 63, 344–7 (1941) – in Discussion of "A Study of Circulation in High-Pressure Boilers and Water-Cooled Furnaces."

50. A. P. Fraas, Flow Stability in Heat Transfer Matrices Under Boiling Conditions, ORNL CF-59-11-1 (Nov. 1, 1959).

51. C. F. Bonilla, op. cit., ref. 46, pp. 333–44.

52. H. A. Roberts, A Flow Stability Criterion for Heated Liquids, paper presented at the E.A.E.S. Symposium on "Heat Transfer Problems in Nuclear Reactors," Karlsruhe (March 1960); communicated to authors by H. A. Roberts, June 1, 1960.

53. M. Altman, "Heat Transfer in Reactors Cooled and Moderated by Water," Nucleonics 66, 68–73 (1956).

54. J. B. Reynolds, Local Boiling Pressure Drop, ANL-5178 (March 1954).

55. J. H. Bick, A New Method for Determining the Stability of Two-Phase Flow in Parallel Heated Channels with Applications to Nuclear Reactors, NAA-SR-4927 (Atomics International) (May 1, 1960); reported in Power Reactor Technology 3, No. 4, 31–32 (1960).

56. W. R. Gambill, TSR-II Fluid Flow Studies, ORNL CF-59-10-104 (Oct. 21, 1959).

57. W. R. Gambill and R. D. Bundy, Burnout Heat Fluxes for Low-Pressure Water in Natural Circulation, ORNL-3026 (Dec. 20, 1960).

58. W. R. Gambill and R. D. Bundy, originally reported as HFIR Natural-Circulation Heat-Transfer Tests in Air, internal memorandum to C. E. Winters, Nov. 2, 1960.

59. W. R. Gambill and R. D. Bundy, originally reported as Permissible Power Level for HFIR Samarium Burnup with Natural-Circulation Heat Removal, internal memorandum to C. E. Winters, Aug. 24, 1960.

60. L. F. Epstein, "Correlation and Prediction of Explosive Metal-Water Reaction Temperatures," Paper 19-8, Trans. Am. Nuclear Soc. 3, No. 2, 431-2 (1960).

61. E. R. G. Eckert and G. M. Low, Temperature Distribution in Internally Heated Walls of Heat Exchangers Composed of Noncircular Flow Passages, NACA-TN-2257, Fig. 7, p. 32 (Jan. 1951); also reported by M. E. Lapides and M. B. Goldstein, Heat Transfer Source File Data, APEX-425, pp. 33-37 (Sept. 1957).

62. J. C. Griess et al., Effect of Heat Flux on the Corrosion of Aluminum by Water. Part II. Influence of Water Temperature, Velocity, and pH on Corrosion-Product Formation, ORNL-3056 (Feb. 10, 1961).

APPENDICES

In these appendices, several miscellaneous experimental and analytical HFIR heat-transfer studies, previously reported orally or in outline form by letter, are presented in greater detail.

Appendix I. Supplementary Burnout Comparisons

Supplementary comparisons between the high-velocity axial-tube-flow burnout data of ref. 5 and four burnout correlations were made with the results outlined in Table 9. An important point illustrated by this comparison concerns the relative effectiveness of various types of burnout correlations when applied to conditions far removed from those of the tests from which they were developed. Equation (27), for example, is statistically derived and represents the data on which it is based[42] within a maximum deviation of 16%. When applied to the data of ref. 5, however, where the velocities are much higher and the heated lengths considerably shorter, the agreement between prediction and experiment is poor. The arbitrary statistical nature of the 24-term Jacobs-Merrill burnout equation[15] illustrates the point even better, since the data of ref. 5 are in disagreement with its predictions by more than 1000% at the highest velocities, where test conditions were such that only the tube diameter was in the recommended variable range for the correlation. The Povarin-Semenov equation,[43] on the other hand, was developed specifically for high velocity conditions and gives good agreement with the data, especially when the constant is increased by 19%, as in Eq. (29). In the original paper, the method was recommended for P = 500 to 600 psia and appeared to be most accurate for velocities greater than 45 fps, in which range the maximum error was 22%.

The generalized, semitheoretical correlation of Griffith[18] is based on a burnout model and appears to be considerably more satisfactory over a very broad variable range than the statistical correlations. Griffith's equation also yields predictions in good agreement with limited burnout data for nonaqueous fluids — benzene, n-heptane, n-pentane, and ethanol,

Table 9. Supplementary Comparisons of Four Burnout Correlations with High-Velocity Burnout Data for Tube Flow from Ref. 5

Eq. No.	Proponents	Correlation[a]	Variable Ranges	Reference	Error[b] (%)		
					Minimum	Average	Maximum
27	Mirshak, Durant, and Towell	$\phi_{bo} = 479{,}000\ (1 + 0.0365\ V) \times$ $\times\ (1 + 0.00507\ \Delta t_{sub})(1 + 0.0131\ P)$	D_e = 0.21–0.46 in. L_h = 19–24 in. P = 25–85 psia Δt_{sub} = 9–135°F V = 5–45 fps (65 tests)	42	34.2	49.5	77.6
6	Griffith	← See Table 6, Eq. (6) →		18	17.7	37.4	55.6
9	Zenkevich and Subbotin	$\phi_{bo} = 396\ G^{0.5}\ \Delta t_{sub}^{0.33} \left(\frac{\rho_l - \rho_v}{\rho_l}\right)^{1.8}$	(See Table 6)	21, 22	2.0	21.5	70.4
28	Povarin and Semenov	$\phi_{bo} = 985{,}000\ (1 + 0.00945\ \Delta t_{sub}) \times$ $\times\ [(V + 26.2)/26.2]^{0.8}$	D_i = 0.045–0.118 in. L_h = 0.315–1.575 in. P = 514 psia Δt_{sub} = 0–362°F V = 11.8–147.7 fps (31 tests)	43	8.5	24.2	39.0
29[c]	Povarin and Semenov	Eq. (13) with constant of 985,000 changed to 1.17×10^6		43	2.7	17.1	52.5

[a] Units in equations are Btu/hr·ft², fps, lb/hr·ft², °F, and psia.

[b] Axial-flow data used in comparison taken from ref. 5 (p. 21, Table 2, tests 1 through 22), for which V_2 = 24 to 174 fps, P_2 = 10 to 74 psia, $(\Delta t_{sub})_2$ = 78 to 222°F, D_i = 0.18 and 0.31 in., and $\phi_{bo} = 2.23 \times 10^6$ to 17.25×10^6 Btu/hr·ft². Error computed as calculated minus experimental, divided by experimental, times 100.

[c] Constant of Eq. (28) changed by authors to obtain best fit with data of ref. 5.

for example. The Zenkevich-Subbotin equation again gives a reasonably good account of itself, especially in view of its simplicity and the fact that the pressures are much lower and the velocities generally much higher than in the tests from which it was developed.

Appendix II. HFIR Minimum Shutdown Flow Rate

A theoretical and experimental study was made of the minimum forced-convection downflow rates permissible for afterheat removal following core shutdown.

Theoretical

Two cases were considered: the first was based on ϕ_a = 61,000 Btu/hr·ft^2, P_2 = 500 psia, and t_{b_1} = 120°F; and the second was based on ϕ_a = 45,000 Btu/hr·ft^2, P_2 = 27 psia (pool head only), and t_{b_1} = 120°F. The afterheat flux estimates of Hilvety[44] predict a maximum fuel-plate heat flux at the inner radius of the fuel annulus of 42,000 Btu/hr·ft^2 at 1.0 sec. Six failure or instability and three supplementary criteria were applied with the following results:[45]

	Criterion	$(V_1)_{min}$ (fps) Case 1	Case 2
1.	Steady-flow burnout	0.65	0.95
2.	$\overline{Gr}/\overline{Ka}$ = 2	0.85	(0.71)
3.	Inception of local boiling	0.83	1.44
4.	Inception of bulk boiling	0.65	1.10
5.	Positive slope of W-ΔP curve (based on local boiling)	0.62	1.13
6.	Positive slope of W-ΔP curve (based on bulk boiling)	0.59	1.11
7.	$(t_w)_{max}$ = 400°F	1.12	(bo at ~305°F)
8.	$(Re)_m = 4 \times 10^3$	1.78	1.62
9.	dt same as in normal operation (65°F)	2.86	2.11

The steady-flow burnout values were calculated with Eq. (10).

The theoretical criterion[46] that coolant downflow with thermal buoyancy is metastable if

$$\frac{\overline{Gr}}{\overline{Ka}} = \frac{\rho^2 \beta g (dt) D_e}{4fG^2} > 2 \qquad (30)$$

applies only to a single-phase coolant; since bulk boiling occurs at a higher velocity in case 2, the criterion is irrelevant in that case. The variation of the dimensionless ratio $\overline{Gr}/\overline{Ka}$ with V is shown for the two cases in Fig. 22.

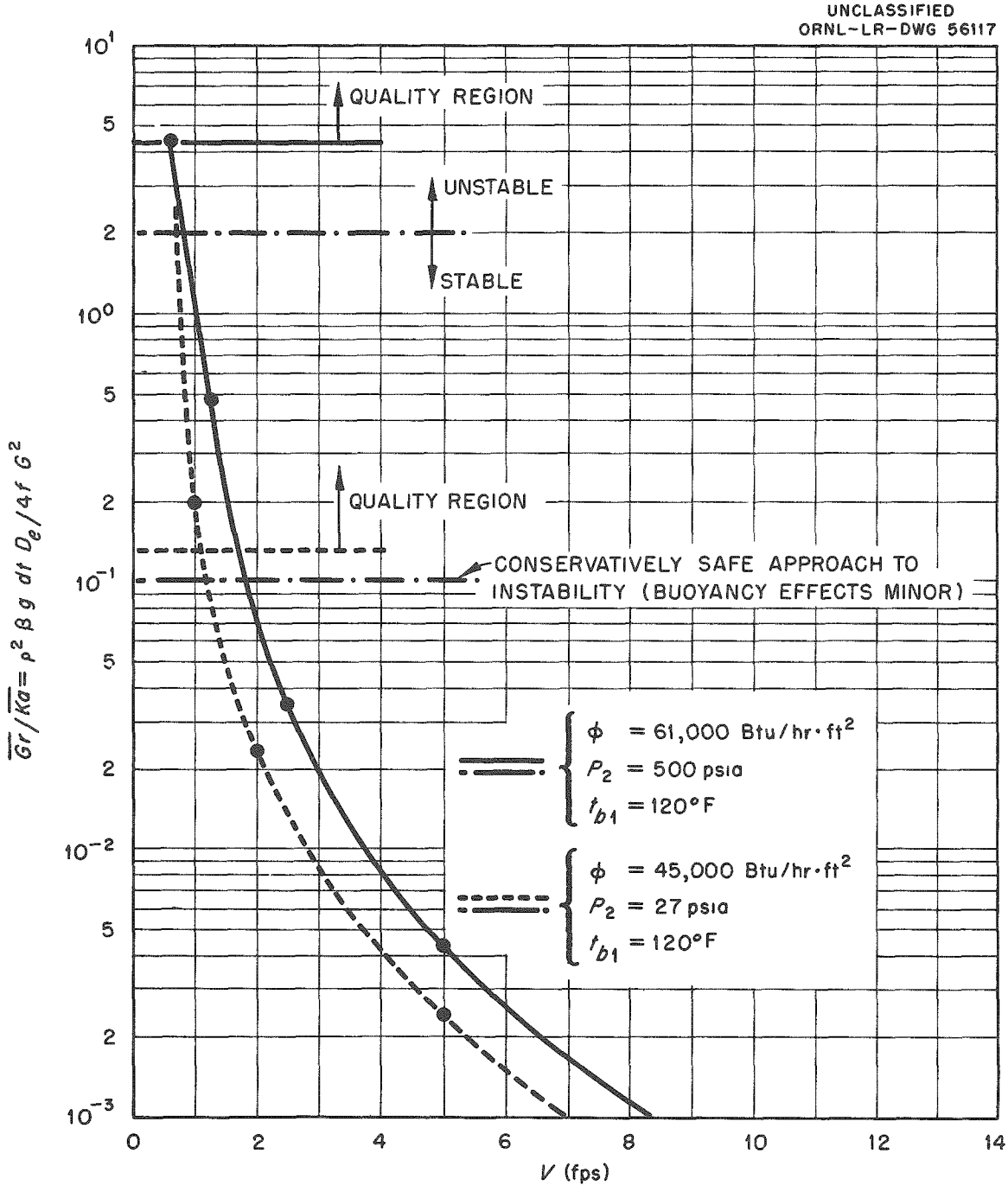

Fig. 22. HFIR Downflow Stability with Afterheat, $\overline{Gr}/\overline{Ka}$ vs V.

Criterion 3 – the inception of local boiling – was estimated by iteratively calculating the flow velocity at which $(t_w)_{nb}$, calculated from

$$(t_w)_{nb} = t_b + \Delta t_f = t_b + \frac{\phi}{h_{nb}} \quad , \tag{31}$$

equalled the local-boiling wall temperature, $(t_w)_{lb}$, calculated from the Jens and Lottes relation[47]

$$(t_w)_{lb} = t_{sat} + \frac{60\ (\phi/10^6)^{1/4}}{\exp\ (P/900)} \quad , \tag{32}$$

at the end of the channel. A graphical application of this method, whereby the initiation of local boiling is found graphically as the intersection of the lines $(t_w)_{nb}$ versus x and $(t_w)_{lb}$ versus x, is given in ref. 48. The criterion of bulk-boiling inception was calculated as the velocity at which $t_{b_2} = t_{sat}$ at P_2.

Criteria 5 and 6 are based on a general examination of the variation of pressure drop with flow rate in a single heated channel. Figures 23 and 24 show this variation as calculated for afterheat cases 1 and 2 with the homogeneous-flow method of Leib,[49] as restated by Fraas.[50] Other material concerning this approach to two-phase flow stability may be found in discussions by Bonilla,[51] Roberts,[52] and Altman.[53] As the flow rate is decreased, ΔP also initially decreases; but with a simultaneously increasing water temperature, local boiling begins near the flow exit (point a). With further lowering of the flow rate, local boiling occurs over a greater fraction of the heated length, and ΔP decreases at an increasingly slower rate. The dotted curves, which indicate modifications of the solid curves due to local boiling, were calculated with Reynolds' method.[54] An additional flow decrease brings the exit water to saturation, and bulk boiling begins at point b. Further decreases in W produce increased ΔP's up to point d, after which the effect of smaller flow rates overtakes the effects of increased specific volumes, and ΔP's decrease with decrease of W once more, the curve merging asymptotically with the single-phase vapor

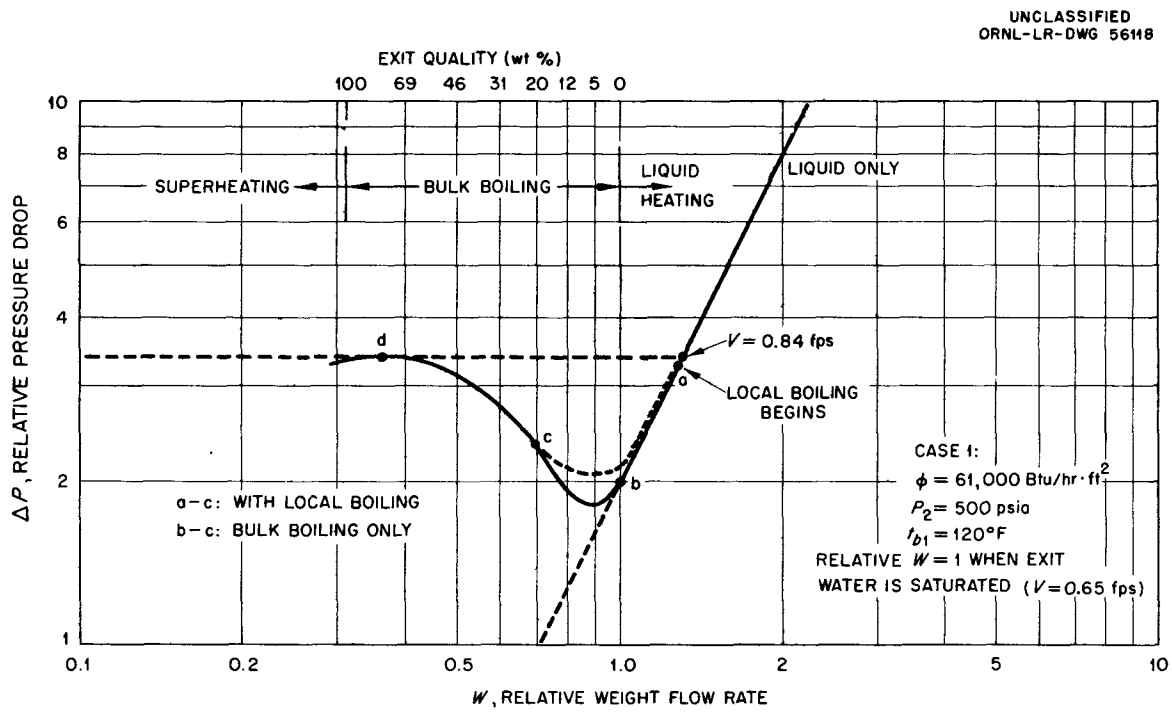

Fig. 23. Flow Rate-Pressure Drop Relation for the HFIR, Afterheat Case 1.

flow curve. As pointed out in detail in refs. 48 through 53, operation in a region where $d(\Delta P)/dW$ is negative is likely to be dangerous, whereas a positive value of $d(\Delta P)/dW$ indicates stability. A more recent stability analysis developed by Bick[55] predicts that if all the terms $\partial(\Delta P_f)_i/\partial G_i$ for a core are positive, flows will be stable; and if two or more of the partial derivatives are negative, flows will be unstable. If, however, only one of the derivatives is negative, the flows may or may not be stable, depending upon design conditions. In the partial derivative, $(\Delta P_f)_i$ is the frictional ΔP in the ith channel, and G_i is the coolant mass velocity in that channel.

Supplementary criteria 7 through 9 are of secondary interest. Number 7 was calculated with the heat-transfer-coefficient correlations presented previously. Number 8 was based on the possibility that some pulsation of the flow rate could occur if operation were in the transition flow regime; though such is the case for tubes, other studies[56] indicate that such pulsations are very mild or nonexistent for parallel-plate channels.

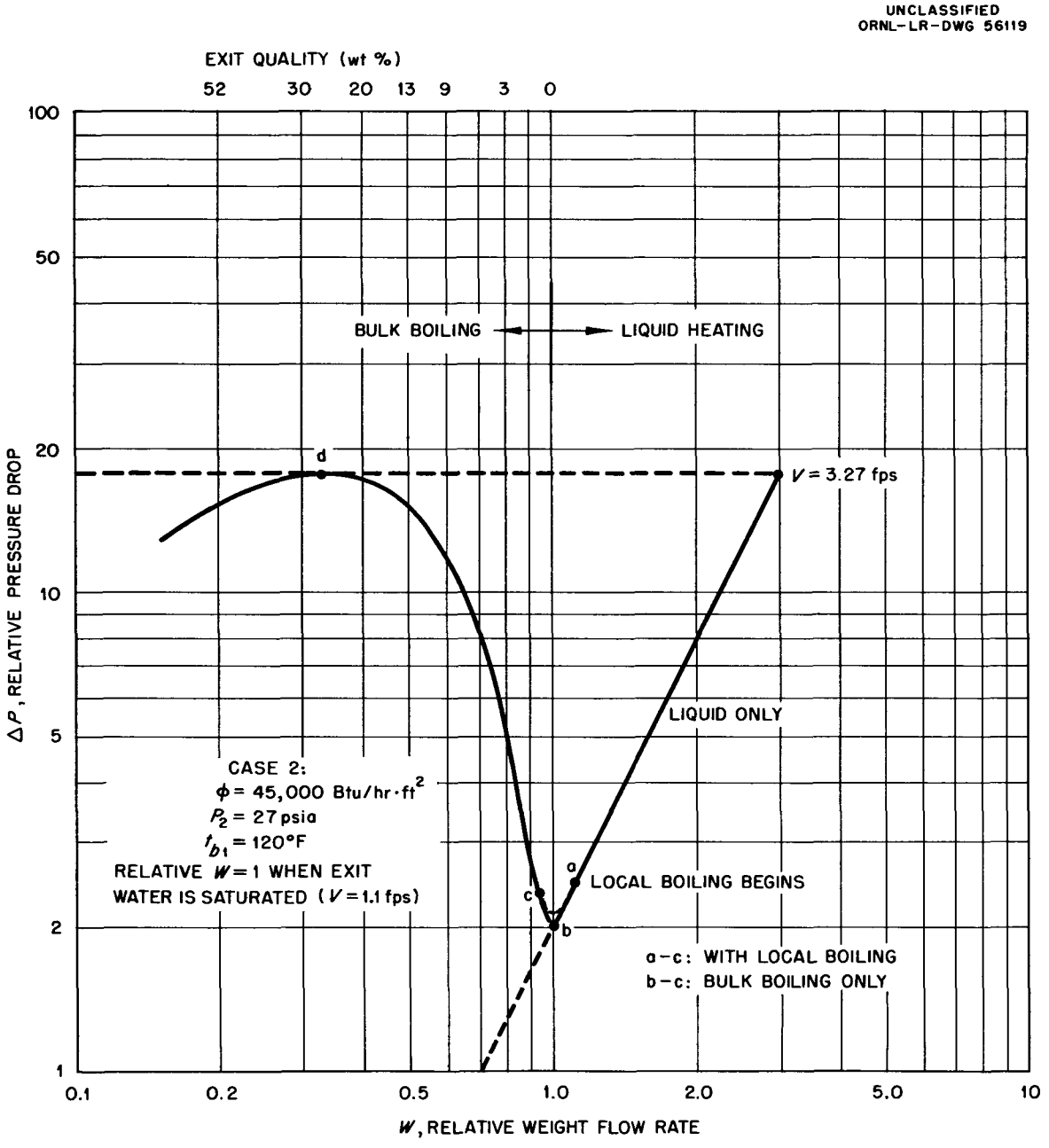

Fig. 24. Flow Rate-Pressure Drop Relation for the HFIR, Afterheat Case 2.

Criterion No. 9 is based on a 65°F coolant temperature rise to give the same axial thermal stresses as in normal 100-Mw operation. It was also calculated by a criterion similar to Eq. (30) that if the velocity were constantly reduced in proportion to the temporal decrease of thermal power

(to keep dt constant at 65°F as the power changed), the minimum stable downflow velocity would be 0.20 fps.

Experimental

Two tests were conducted with 18-in.-long aluminum test sections heated electrically and cooled by a decreasing water downflow at nearly constant ϕ. Test 1, approximating case 1 conditions, was made with ϕ = 76,500 Btu/hr·ft^2 (at burnout), P_2 = 515 psia, and t_{b_1} = 117°F. Coolant velocity at incipient burnout was 0.75 fps, and $(t_w)_{max}$ attained 400°F at V_1 = 1.10 fps. The complete data from both tests are shown in Fig. 25. The agreement with the predictions is considered satisfactory for each criterion. Test 2, approximating case 2 conditions, was conducted with ϕ = 40,800 Btu/hr·ft^2 (at burnout), P_2 = 27.1 psia, and

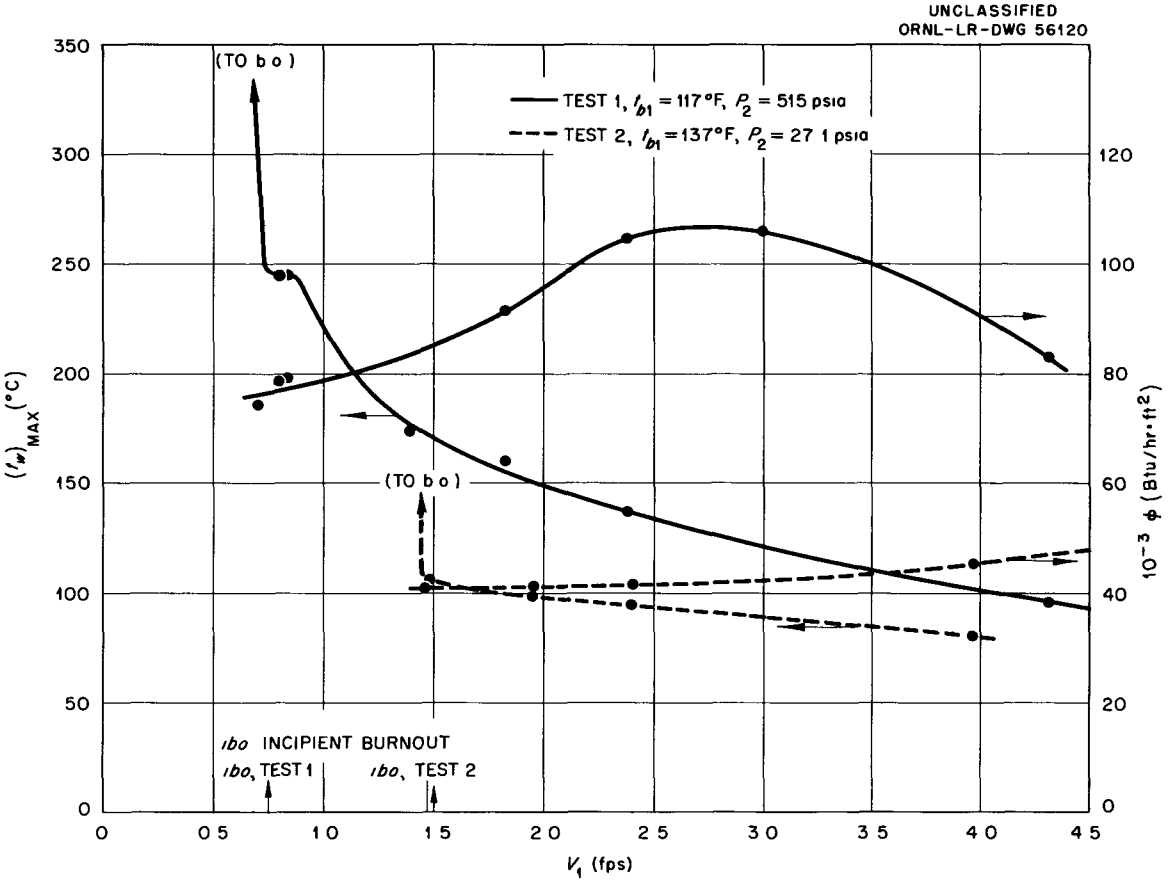

Fig. 25. Variation of Maximum Surface Temperature in HFIR Minimum Downflow Tests.

t_{b_1} = 137°F. Coolant velocity at incipient burnout was 1.48 fps. Inlet-water temperature variations rather strongly affect the burnout velocity in the low-pressure case (by causing a large fractional change in the exit Δt_{sub}), and the observed V_{bo} is in good agreement with prediction (2%) when the warmer inlet water of the experiment is taken into account.

It may be concluded that a minimum shutdown flow rate of 5% (V = 2 fps) would be safe. This estimate includes an average/minimum coolant velocity factor of 1.08. The proposed 10% shutdown flow rate will be conservatively safe, according to all the thermal and flow criteria employed. The burnout safety factor, e.g., is ~27, and the coolant temperature rise is less than that corresponding to normal full-power operation.

Appendix III. Additional Natural-Circulation Studies

Measurements of burnout heat fluxes, surface temperature distributions, and flow oscillations – and correlations for burnout heat flux – have been reported[57] for natural-circulation flow in both HFIR and other geometries. The results of two other natural-circulation studies[58,59] which have been made in the meantime are presented here.

HFIR Natural-Circulation Heat Transfer to Air

A series of six tests was made in order to determine the heat-transfer capabilities of a vertically oriented HFIR aluminum test section in an essentially infinite environment of atmospheric air. The tests were motivated by a desire to determine the heat flux which would produce a maximum metal temperature of 1020°F – that is, 200°F below the melting point and the maximum permissible in the event of an accident during shipment of a used fuel-element assembly.

The heated length of the test section was 18 in.; total length, 21 in.; average flow gap, 0.052 in.; and average gap width, 0.499 in. Outer surface temperatures, which were recorded at various heat fluxes with twelve Chromel vs Alumel thermocouples located on both front and rear faces, approached their equilibrium values slowly because of heat-capacity lag. Several hundred recording cycles were usually required for the temperature-time curves to approach a slope of zero. Equilibrium temperatures were calculated by extrapolating the measured values to infinite time – that is, to a zero value of the reciprocal of the number of cycles.

The results of this experiment are plotted in Fig. 26. The values corresponding to the line drawn through the data points are:

Corrected ϕ (Btu/hr·ft^2)	$(t_{surface})_{max}$ (°F)
0	79
1×10^3	298
2×10^3	491
3×10^3	667
4×10^3	837
5×10^3	997
5.15×10^3	1020
6.70×10^3	1220 (m.p.)

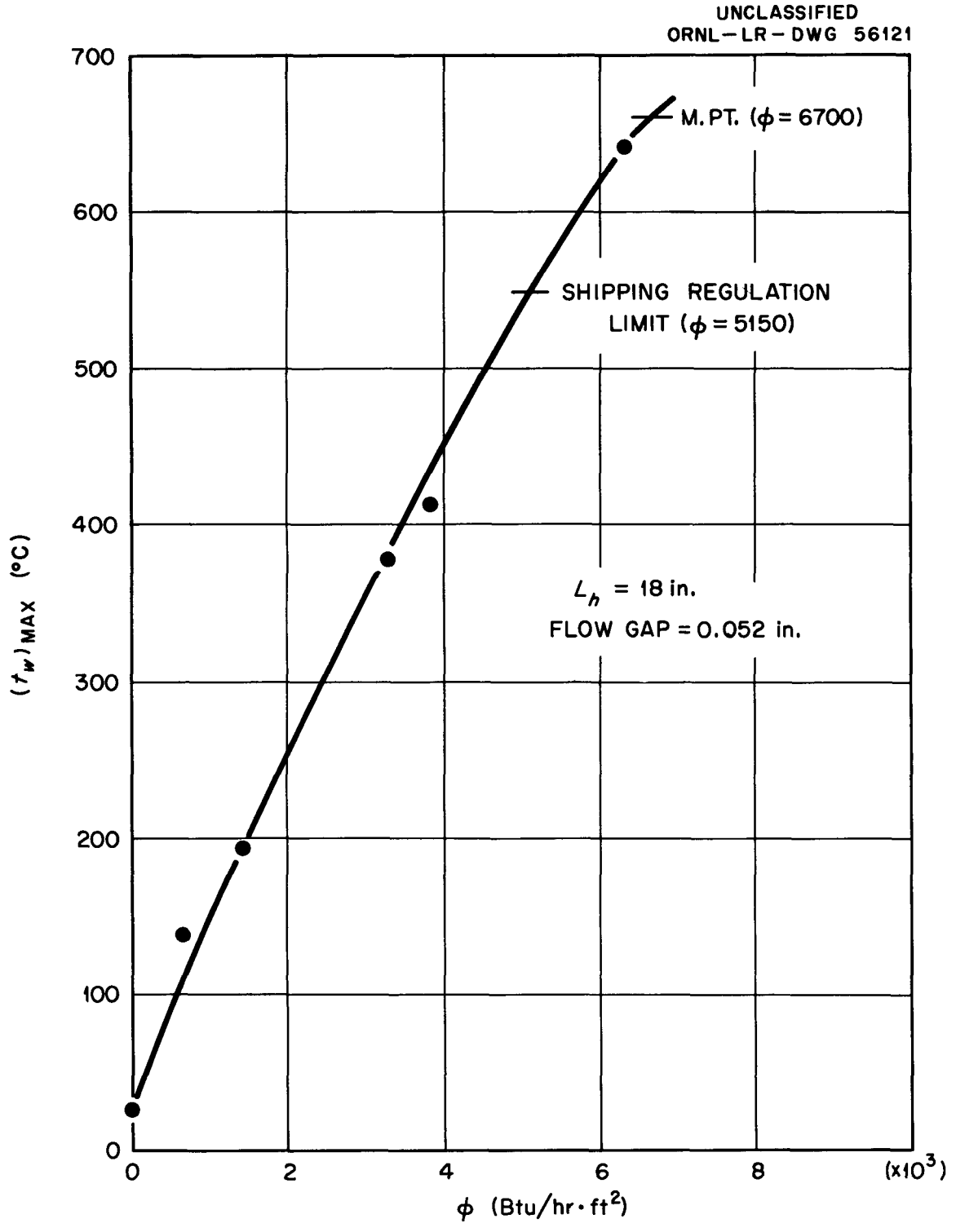

Fig. 26. Maximum Surface Temperature vs Heat Flux for Natural Circulation of Atmospheric Air Through a Vertical HFIR Test Section.

According to the HFIR afterheat flux estimates of Hilvety,[44] a maximum fuel-plate ϕ of 5150 Btu/hr·ft^2 will be reached approximately 1 hr and 35 min after core shutdown.

The occurrence of the highest measured temperatures toward the center of the test section was an indication of the relative importance of radiative heat transmission for this case. The calculated maximum conduction rate to the ends of the aluminum section was 7% of the generation rate. The maximum aluminum oxide thickness at the end of the test was reported to be 0.07 mils, which corresponds to a maximum temperature correction of 5°F.

Permissible Power Level for HFIR Samarium Burnup with Natural-Circulation Heat Removal at Low Pressure

In order to fix the length of time necessary for samarium burnup in a partially used HFIR core, calculations were made to determine the power level at which water in natural circulation under pool head would exit from an HFIR core at the saturation temperature. The following values were fixed:

Active fuel-plate length	18 in.
Total fuel-plate length	24 in.
Flow gap	0.050 in.
Control plate extensions	3 ft at each end
Submergence of top of core beneath pool surface	17 ft
Height of bottom of core above bottom of pool	5 ft
Fuel-annulus inside diameter	5.444 in.
Fuel-annulus outside diameter	15.712 in.
Metal-to-water ratio	1.0
Pool water temperature	110°F (max)
Hot-channel average heat flux	1.42 times core-average heat flux

The island heat load was neglected.

If it is assumed that the average exit fluid temperature is equal to t_{sat}, a power level of 4.0 Mw is required. The hot channels, however, would produce net steam (~5.4 wt % quality at exit). Consideration of all pressure losses – contraction, expansion, turning, acceleration, and friction – gives an upward water velocity of 0.95 fps, which corresponds to laminar flow. The upper 3-ft-long control-cylinder extension would act effectively as a draft tube, since heat-loss calculations for the cylinder indicate that the maximum decrease of core-exit water temperature across the 3-ft-exit length would be only 1.1°F.

If it is assumed that the hot-channel exit water is saturated, the average water velocity decreases to 0.67 fps and 2.0 Mw are required to establish the assumed condition. Water leaving the average channels would be subcooled in this instance by 36°F.

Appendix IV. Aluminum-Water Reaction Tests

In the early stages of the experimental program, there was some concern over the possibility of a violent Al-H_2O chemical reaction at burnout. A series of three qualitative tests was conducted, wherein a type 1100 aluminum tube was filed to one-half its initial diameter (1/8 in.) over a 1-in. length in order to locally peak the heat flux. The tube was connected to electrodes and submerged in water in an open 55-gal drum, in the manner sketched below:

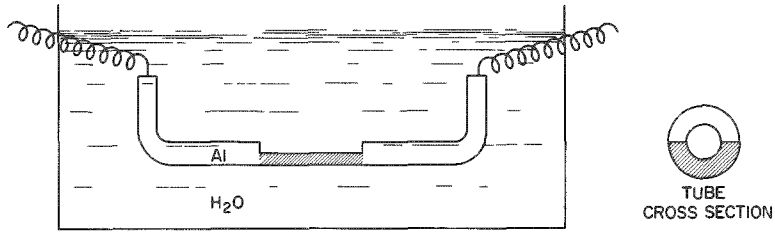

The system was visually observed from above with a suspended mirror as the current through the tube was gradually increased with a Variac until failure occurred. In stagnant water, the failure phenomenon was very quiet, and no flash was visible. When water was directed over the 1-in. length at ~6 fps with a small propeller mixer, the failure was loud and the flash visible. A 40-fps jet from a copper tube produced a quite loud failure and an accompanying bright flash. The observations seemed reasonable, since increased velocities allow greater heat fluxes and therefore increased energy storage rates in the metal before burnout, as well as increasing the chance that a water eddy will penetrate the steam layer to the molten metal surface at burnout. It was concluded that the reaction would not be an experimental problem. A safety shield was used, but no violent chemical effects were noted in any of the tests.

In the most recent study of metal-water reactions,[60] Epstein indicates that explosive reactions require that the metal be above its melting point and in a finely divided form (droplet diameters $\leq 500\ \mu$). For aluminum, the explosive reaction temperature is given as 1170°C (2138°F).

Appendix V. Approach of Fuel Meat to Side Plates

It is undesirable to extend the fuel alloy in the fuel plates all the way to the side plates, since decreased velocities and heat-transfer coefficients in the corners would lead to significantly increased metal temperatures. Estimates of the permissible fuel-meat approach were made with the analytical predictions of Eckert and Low[61] for the local heat-transfer coefficients in corners of noncircular flow passages. This analysis, which is based on turbulent flow of a fluid with a Prandtl number of unity and on equality of the eddy diffusivities of heat and momentum transfer, gives the following variation of the minimum distance from the corner (x) with the angle subtended by the sides of the corner (β) if the local h is to be 0.8 of the channel-average h:

β (deg)	x/D_e	Corresponding HFIR x (mils)
90	0.034	3.4
60	0.081	8.1
45	0.257	25.7
30	0.470	47.0

The Prandtl number of the HFIR cooling water is 2.8 at $(t_b)_m$ and 1.7 at $(t_b)_{2,max}$, or probably close enough for the analysis to apply with sufficient accuracy. The analysis has been confirmed within ~20%, with a few data for heating air in noncircular ducts. Since the angle between the outer edges of the fuel plates and the side plates in the inner and outer fuel annuli are 32.70 deg and 44.75 deg, respectively, it was decided to limit the minimum radial approach of the fuel meat to 1/16 in.

ORNL-3079

UC-80 — Reactor Technology
TID-4500 (16th ed.)

INTERNAL DISTRIBUTION

1. L. G. Alexander
2. C. F. Allen (K-25)
3. E. S. Bettis
4. D. S. Billington
5. F. T. Binford
6. E. P. Blizard
7. A. L. Boch
8. C. J. Borkowski
9. G. E. Boyd
10. R. B. Briggs
11-21. R. D. Bundy
22. C. A. Burchsted
23. C. E. Center (K-25)
24. T. G. Chapman
25. R. A. Charpie
26. R. D. Cheverton
27. H. C. Claiborne
28. R. S. Cockreham
29. T. E. Cole
30. C. W. Collins
31. J. W. Cooke
32. F. L. Culler
33. E. P. Epler
34. W. K. Ergen
35. A. P. Fraas
36. J. L. Fowler
37. J. H. Frye, Jr.
38. W. R. Gall
39-74. W. R. Gambill
75. W. F. Gauster
76. J. P. Gill
77. J. C. Griess
78. W. R. Grimes
79. E. Guth
80. L. A. Haack
81. D. C. Hamilton
82. R. J. Hefner
83. R. L. Higgins (K-25)
84. N. Hilvety
85-88. H. W. Hoffman
89. A. Hollaender
90. L. B. Holland
91. A. S. Householder
92. W. H. Jordan
93. P. R. Kasten
94. C. P. Keim
95. M. T. Kelley
96. J. J. Keyes, Jr.
97. G. J. Kidd, Jr.
98. W. Kofink
99. A. I. Krakoviak
100. P. G. Lafyatis
101. J. A. Lane
102. C. G. Lawson
103. J. S. Lewin
104. R. S. Livingston
105. J. Lones
106. M. I. Lundin
107. F. E. Lynch
108. R. N. Lyon
109. H. G. MacPherson
110. W. D. Manly
111. E. R. Mann
112. M. M. Martin
113. T. H. Mauney
114. H. A. McLain
115. J. R. McWherter
116. J. W. Michel
117. A. J. Miller
118. C. S. Morgan
119. K. Z. Morgan
120. M. L. Nelson
121. L. C. Oakes
122. J. J. Perona
123. A. M. Perry
124. D. Phillips
125. C. A. Preskitt
126. M. E. Ramsey
127-128. P. M. Reyling
129. M. W. Rosenthal
130. G. Samuels
131. H. C. Savage
132. A. W. Savolainen
133. H. E. Seagren

134. E. D. Shipley
135. M. J. Skinner
136. A. H. Snell
137. I. Spiewak
138. W. J. Stelzman
139. R. S. Stone
140. J. A. Swartout
141. E. H. Taylor
142. D. G. Thomas
143. M. Tobias
144. D. B. Trauger
145. J. N. Turpin (Y-12)
146. J. W. Ullmann
147. W. E. Unger
148. D. H. Wallace
149. J. L. Wantland
150. A. M. Weinberg
151. M. E. Whatley
152. C. E. Winters
153. M. M. Yarosh
154-155. Central Research Library
156-175. Laboratory Records Department
176. Laboratory Records, ORNL-RC
177-178. ORNL-Y-12 Technical Library Document Reference Section
179. Reactor Division Library, Bldg. 9204-1, Y-12

EXTERNAL DISTRIBUTION

180. Division of Research and Development, AEC, ORO
181-782. Given distribution as shown in TID-4500 (16th ed.) under Reactor Technology category (75 copies-OTS)